Cell Reports

Article

The ApoA-I mimetic peptide 5A enhances remyelination by promoting clearance and degradation of myelin debris

Graphical abstract

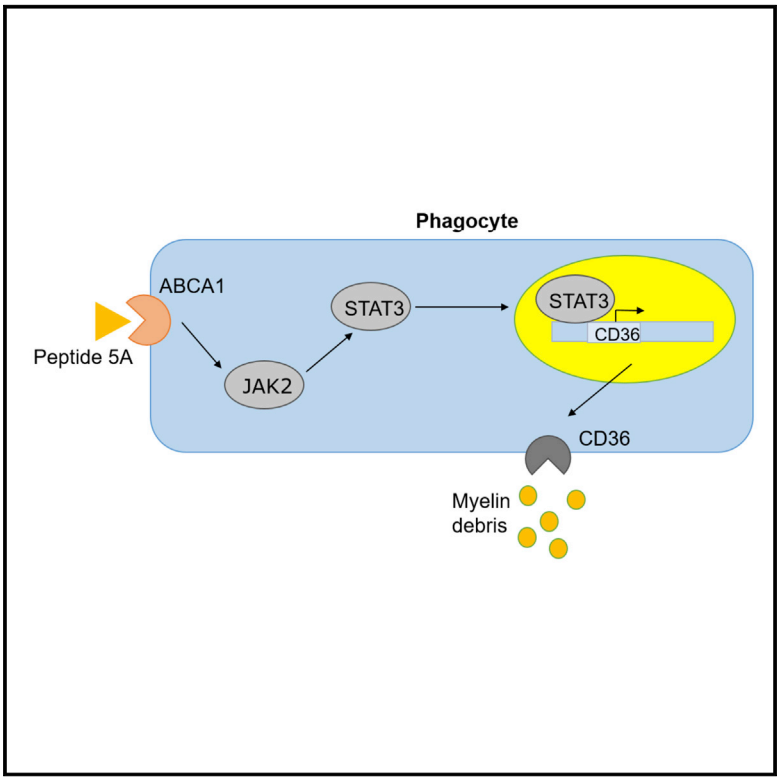

Authors

Sam Vanherle, Winde Jorissen, Tess Dierckx, ..., Mansour Haidar, Jerome J.A. Hendriks, Jeroen J.F. Bogie

Correspondence

jeroen.bogie@uhasselt.be

In brief

Vanherle et al. report that the ApoA-I mimetic peptide 5A enhances central nervous system repair by promoting the clearance and metabolism of myelin debris by macrophages and microglia through the fatty acid translocase CD36. Their findings argue for peptide 5A being a promising therapeutic compound to enhance repair of demyelination.

Highlights

- ApoA-I mimetic peptide 5A enhances remyelination in a phagocyte-dependent manner
- In addition to promoting lipid efflux, peptide 5A enhances clearance of myelin debris
- Peptide 5A drives clearance of myelin debris via the fatty acid translocase CD36

Vanherle et al., 2022, Cell Reports *41*, 111591
November 8, 2022
https://doi.org/10.1016/j.celrep.2022.111591

CellPress

Cell Reports

CellPress
OPEN ACCESS

Article

The ApoA-I mimetic peptide 5A enhances remyelination by promoting clearance and degradation of myelin debris

Sam Vanherle,[1,2] Winde Jorissen,[1,2] Tess Dierckx,[1,2] Melanie Loix,[1,2] Elien Grajchen,[1,2] Fleur Mingneau,[1,2] Jeroen Guns,[1,2] Pascal Gervois,[3] Ivo Lambrichts,[3] Jonas Dehairs,[4] Johannes V. Swinnen,[4] Monique T. Mulder,[5] Alan T. Remaley,[6] Mansour Haidar,[1,2] Jerome J.A. Hendriks,[1,2,7] and Jeroen J.F. Bogie[1,2,7,8,*]

[1]Department of Immunology and Infection, Biomedical Research Institute, Hasselt University, 3590 Diepenbeek, Belgium
[2]University MS Center Hasselt, 3900 Pelt, Belgium
[3]Department of Cardio and Organs Systems, Biomedical Research Institute, Hasselt University, 3590 Diepenbeek, Belgium
[4]Department of Oncology, Laboratory of Lipid Metabolism and Cancer, Leuven Cancer Institute, University of Leuven, 3000 Leuven, Belgium
[5]Department of Internal Medicine, Erasmus University Medical Center, 3015 Rotterdam, the Netherlands
[6]Lipoprotein Metabolism Laboratory, Translational Vascular Medicine Branch, National Heart, Lung, and Blood Institute, National Institutes of Health, Bethesda, MD 20892, USA
[7]These authors contributed equally
[8]Lead contact
*Correspondence: jeroen.bogie@uhasselt.be
https://doi.org/10.1016/j.celrep.2022.111591

SUMMARY

The progressive nature of demyelinating diseases lies in the inability of the central nervous system (CNS) to induce proper remyelination. Recently, we and others demonstrated that a dysregulated innate immune response partially underlies failure of CNS remyelination. Extensive accumulation of myelin-derived lipids and an inability to process these lipids was found to induce a disease-promoting phagocyte phenotype. Hence, restoring the ability of these phagocytes to metabolize and efflux myelin-derived lipids represents a promising strategy to promote remyelination. Here, we show that ApoA-I mimetic peptide 5A, a molecule well known to promote activity of the lipid efflux transporter ABCA1, markedly enhances remyelination. Mechanistically, we find that the repair-inducing properties of 5A are attributable to increased clearance and metabolism of remyelination-inhibiting myelin debris via the fatty acid translocase protein CD36, which is transcriptionally controlled by the ABCA1-JAK2-STAT3 signaling pathway. Altogether, our findings indicate that 5A promotes remyelination by stimulating clearance and degradation of myelin debris.

INTRODUCTION

Failure of remyelination, the formation of myelin sheaths around demyelinated axons, underlies the progressive nature of demyelinating diseases. The current hypothesis states that remyelination is hampered by inefficient recruitment of oligodendrocyte precursor cells (OPCs) to the lesion site, along with a decreased capacity of these cells to differentiate into mature, myelinating oligodendrocytes (Franklin and Ffrench-Constant, 2017; Stangel et al., 2017). While the underlying cause of perturbed OPC recruitment and differentiation is poorly understood, emerging evidence indicates that factors to which OPCs are exposed in demyelinating lesions play an essential role in this impairment (Dillenburg et al., 2018; Keough et al., 2016; Lampron et al., 2015). We and others have demonstrated that inefficient remyelination is in part due to a dysfunctional innate immune response in the central nervous system (CNS) (Bogie et al., 2020; Cantuti-Castelvetri et al., 2018; Marschallinger et al., 2020). More specifically, while macrophages and CNS-resident microglia can display pro-regenerative properties through the release of trophic factors and clearance of myelin debris (Berghoff et al., 2021; Bogie et al., 2012, 2013; Boven et al., 2006), this protective phenotype is only temporary and does not allow remyelination on the long term. With respect to the latter, sustained internalization of myelin induces a harmful phagocytic phenotype that suppresses CNS repair (Bogie et al., 2020). An inability of phagocytes to process myelin-derived lipids, leading to incessant accumulation of myelin-derived cholesterol and formation of lipid droplets, underlies the induction of this disease-promoting phagocytic phenotype (Bogie et al., 2020; Cantuti-Castelvetri et al., 2018; Marschallinger et al., 2020). Therefore, restoring the ability of phagocytes to degrade and dispose of myelin-derived cholesterol and lipid droplets is considered to be a promising therapeutic strategy to promote remyelination.

Cellular lipid metabolism is a tightly regulated process involving a balanced uptake, synthesis, and efflux of lipids. The ATP-binding cassette transporter A1 (ABCA1) is crucial in controlling intracellular lipid content by promoting efflux of

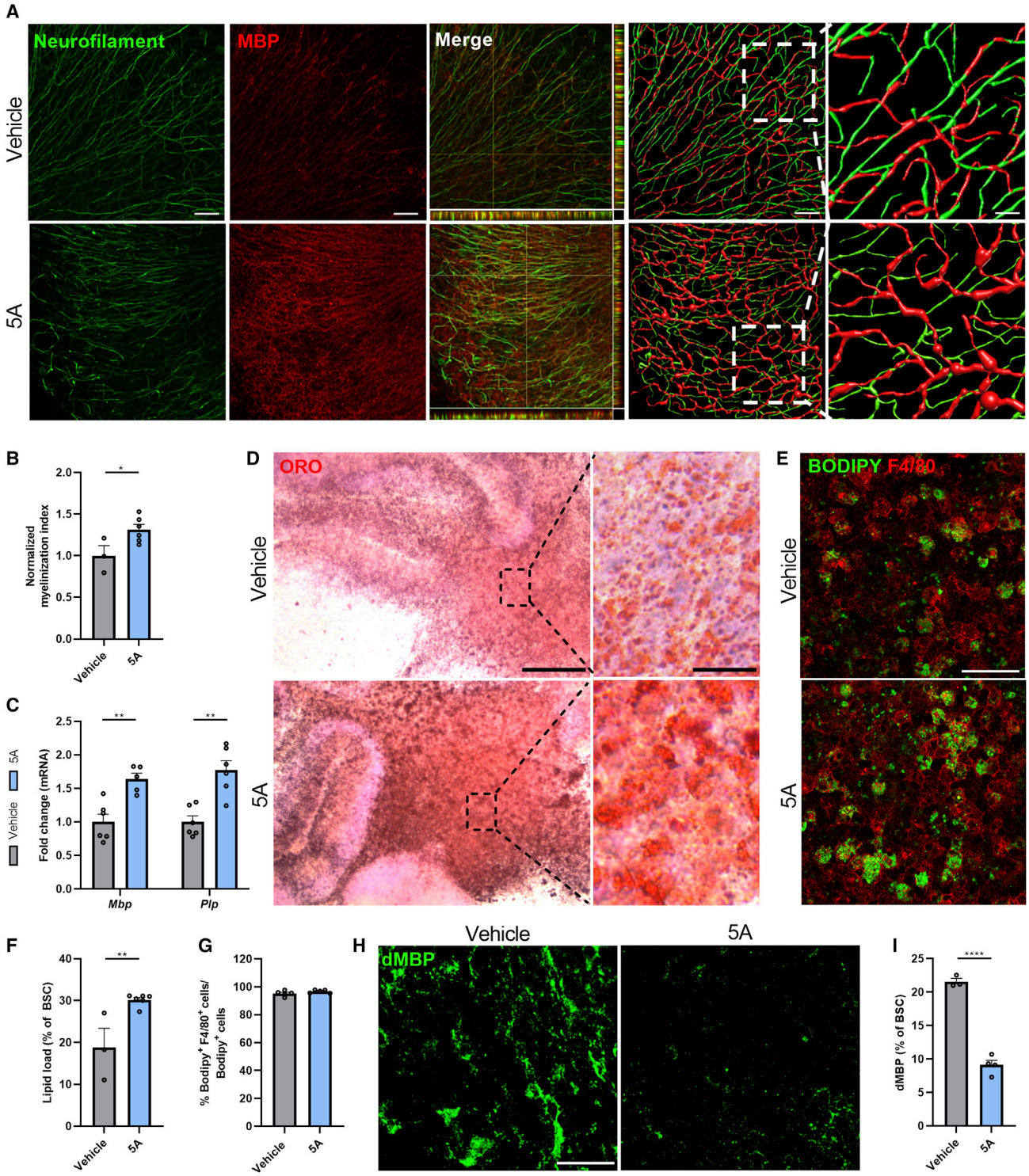

Figure 1. Peptide 5A improves remyelination in the cerebellar brain slice model

(A) Representative images, orthogonal projections (columns 1–3), and three-dimensional reconstruction (columns 4 and 5) of immunofluorescence myelin (MBP) and neurofilament staining of cerebellar brain slice cultures treated with vehicle or peptide 5A (50 μg/mL). Scale bars, 50 μm (overview); 20 μm (insets).

(B) Normalized quantification of MBP^+ NF^+ axons out of total NF^+ axons in cerebellar brain slices treated with vehicle or peptide 5A (n = 3–6 slices). Data are presented compared with vehicle.

(C) mRNA expression of *Mbp* and *Plp* in cerebellar brain slice cultures treated with vehicle or peptide 5A (n = 6 slices).

(legend continued on next page)

cholesterol and phospholipids to apolipoprotein A-I (ApoA-I) to produce nascent high-density lipoproteins (HDL) (Chinetti et al., 2001). Given its essential role in promoting ABCA1-mediated lipid efflux, numerous studies have defined the therapeutic applicability of ApoA-I mimetic peptides to reduce foam cell formation in atherosclerosis (Nanjee et al., 1996; Nissen, 2005). Based on excellent CNS pharmacokinetics of ApoA-I mimetic peptides (Button et al., 2019; Swaminathan et al., 2020), we explored in this study whether the ApoA-I mimetic peptide 5A can promote remyelination by reducing phagocyte lipid load. Peptide 5A is a bihelical peptide that recapitulates the α-helical structure of ApoA-I. In addition to promoting lipid efflux, peptide 5A is reported to have potent antiinflammatory, antioxidant, and immunomodulatory properties in *in vitro* and *in vivo* models of atherosclerosis and colitis (Amar et al., 2010; Nowacki et al., 2016; Tabet et al., 2010; Yao et al., 2011). By using cerebellar brain slices and the cuprizone model, we provide evidence that peptide 5A also enhances remyelination. Surprisingly, enhanced remyelination was associated with an increased cellular lipid droplet load in the CNS. Guided by immunohistochemical and lipidomic analysis, we discovered that the pro-regenerative impact of peptide 5A can be attributed to enhanced efflux of cholesterol and an increased uptake of myelin debris by macrophages and microglia through the fatty acid translocase CD36. On a transcriptional level, peptide 5A controlled CD36 expression through the ABCA1-JAK2-STAT3 signaling pathway. Collectively, our findings indicate that peptide 5A promotes the induction of a repair-permissive environment by stimulating the clearance and degradation of inhibitory myelin debris, potentially having broad implications for therapeutic strategies aimed at promoting remyelination in demyelinating pathologies.

RESULTS

Peptide 5A promotes remyelination *ex vivo* and *in vivo* in a phagocyte-dependent manner

Sustained intracellular accumulation of myelin-derived cholesterol and lipid droplets drives macrophages and microglia toward an inflammatory phenotype that suppresses remyelination (Bogie et al., 2020; Cantuti-Castelvetri et al., 2018; Marschallinger et al., 2020). Given that ApoA-I promotes cholesterol efflux and, in doing so, reduces intracellular lipid droplet load (Chinetti et al., 2001; Nanjee et al., 1996; Nissen, 2005), we reasoned that the application of ApoA-I mimetic peptides could be an effective therapeutic approach to promote remyelination. Remyelination efficacy was first studied using *ex vivo* cerebellar brain slices demyelinated with lysolecithin and treated with the ApoA-I mimetic peptide 5A (experimental design, Figure S1A). Immunohistochemical staining demonstrated increased colocalization of myelin (MBP) and axons (neurofilament) in brain slices treated with peptide 5A (Figures 1A and 1B), indicating more efficient remyelination in peptide 5A-exposed brain slices. Enhanced remyelination was confirmed by orthogonal projections and three-dimensional reconstructions (Figure 1A). Consistent with enhanced remyelination, peptide 5A increased mRNA expression of myelin proteins, i.e., *Mbp* and *Plp* (Figure 1C). Of note, brain slices that were demyelinated with lysolecithin in the presence of peptide 5A showed a similar myelination index, suggesting that peptide 5A does not protect against demyelination (Figure S1B). Counterintuitively, improved remyelination was associated with higher intracellular lipid droplet levels, evidenced by an increased oil red O (ORO) load (Figures 1D and 1F). Of interest, F4/80$^+$ phagocytes were the predominant cell type containing lipid droplets (Figures 1E and 1G). Given that peptide 5A increased cellular lipid droplet load and, at the same time, enhanced remyelination, we assessed whether peptide 5A stimulates remyelination by promoting the clearance of repair-inhibitory myelin debris (Lampron et al., 2015). To this end, we determined the presence of non-cell-associated myelin debris (Grajchen et al., 2020; Miron et al., 2013). Immunohistochemical analysis demonstrated that peptide 5A markedly decreased immunoreactivity for degenerated myelin (dMBP) in remyelinating brain slices (Figures 1H and 1I). These findings indicate that peptide 5A promotes remyelination in the *ex vivo* cerebellar brain slice model and suggest that enhanced clearance of myelin debris underlies the reparative impact of peptide 5A.

To evaluate the significance of these findings *in vivo*, the cuprizone-induced de- and remyelination model was used (experimental design in Figure S1C). Cuprizone feeding leads to reproducible toxic demyelination in distinct brain regions such as the corpus callosum (CC). Cessation of cuprizone administration results in spontaneous remyelination. Similar to the brain slice model, animals treated with peptide 5A showed increased myelin abundance in the CC compared with vehicle-treated animals, both after demyelination (6w) and during remyelination (6w+1; Figures 2A and 2B). In line with the latter, transmission electron microscopy demonstrated that peptide 5A-treated mice displayed a decreased g ratio (the ratio of the inner axonal diameter to the total outer diameter) and an increased percentage of myelinated axons (Figures 2C and 2D). In particular, small-diameter axons showed thicker myelin sheaths in peptide 5A-exposed mice (Figure S1D). Peptide 5A exposure did not lead to changes in axon diameter (Figure S1E). Similarly, quantitative PCR indicated increased *Plp* expression and a trend toward increased *Mbp* expression in the CC of peptide

(D) Representative images of oil red O (ORO) staining of cerebellar brain slice cultures treated with vehicle or peptide 5A. Scale bars, 100 μm (overview); 25 μm (insets).

(E) Representative images of immunofluorescence F4/80 and BODIPY staining of cerebellar brain slice cultures treated with vehicle or peptide 5A. Scale bar, 50 μm.

(F and G) Quantification of the ORO$^+$ area (F; n = 3–6 slices) and percentage BODIPY$^+$ F4/80$^+$ cells/BODIPY$^+$ cells (G; n = 5 slices) of vehicle- and peptide 5A-treated cerebellar brain slice cultures.

(H) Representative images of degenerated MBP (dMBP) staining of cerebellar brain slice cultures treated with vehicle or peptide 5A. Scale bar, 50 μm.

(I) Quantification of the dMBP$^+$ area of vehicle- and peptide 5A-treated cerebellar brain slice cultures (n = 6 slices). Results are pooled from three biological replicates. Data are represented as the mean ± SEM; *p < 0.05; **p < 0.01; ****p < 0.0001. See also Figure S1.

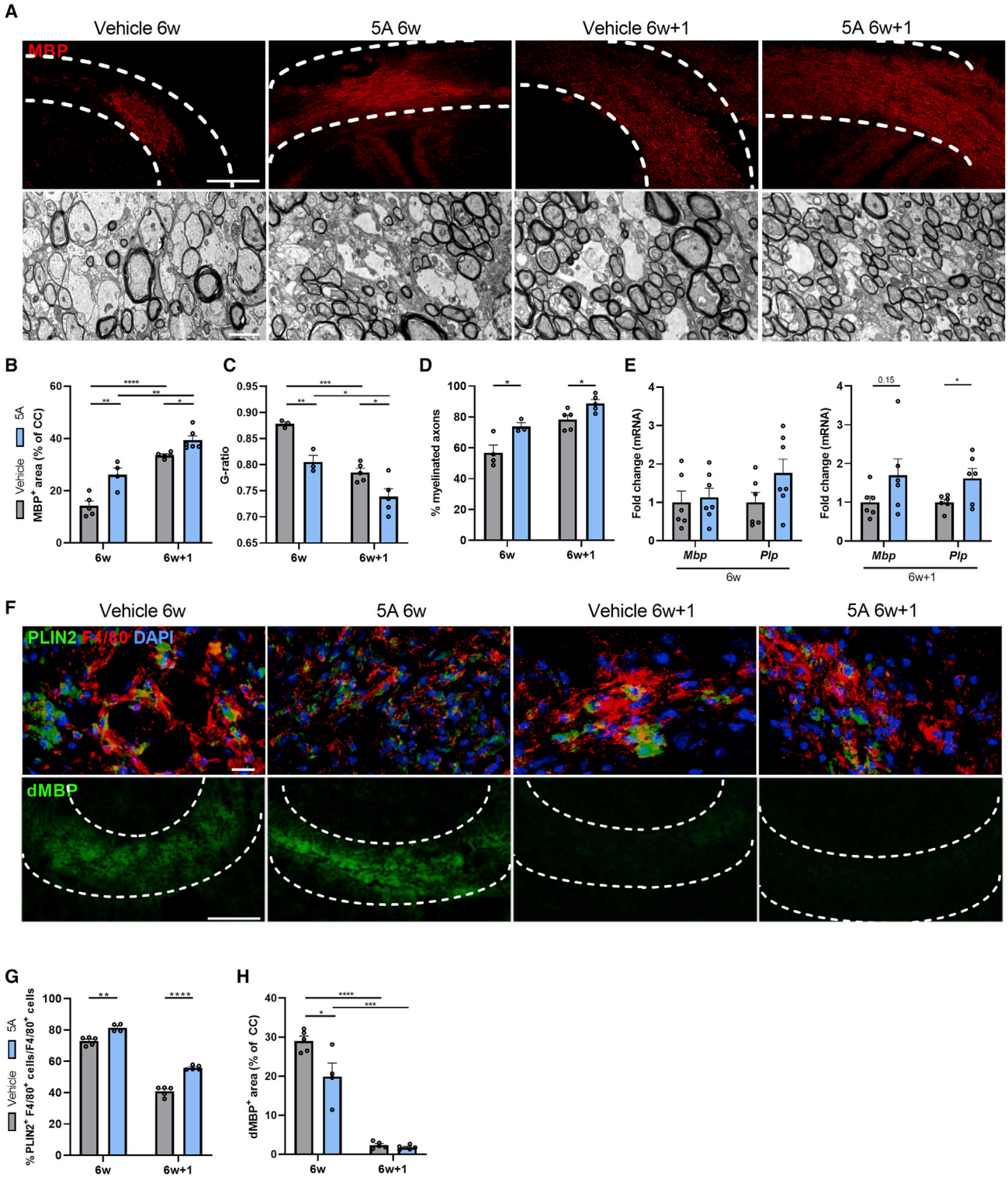

Figure 2. Peptide 5A improves remyelination in the cuprizone model

(A) Representative images of immunofluorescence myelin (MBP) staining and transmission electron microscopy analysis of the corpus callosum (CC) from vehicle- and peptide 5A (30 mg/kg)-treated mice after cuprizone-induced demyelination (6w) and during remyelination (6w+1). Scale bars, 200 μm (top) and 2 μm (bottom).

(B) Quantification of the MBP$^+$ area of the CC from vehicle- and peptide 5A-treated mice after 6w and 6w+1 (n = 4–6 animals).

(legend continued on next page)

5A-treated mice during remyelination (Figure 2E). These results indicate that peptide 5A promotes remyelination *in vivo*. Importantly, also in the cuprizone model, peptide 5A increased cellular lipid droplet load, especially in F4/80$^+$ phagocytes (Figures 2F, 2G, and S1F–S1H), and decreased the presence of degenerated myelin debris (Figures 2F and 2H). Notably, PLIN2$^+$ lipid droplets were primarily present in F4/80$^+$ macrophages and microglia in the CC of vehicle- and peptide 5A-treated mice (Figure S1I). In concordance with enhanced clearance of degenerated myelin debris, electron microscopy analysis showed increased myelin debris-filled vacuoles in phagocytes of peptide 5A-treated mice compared with vehicle-treated mice (Figures S1J–S1K). Although peptide 5A suppresses monocyte infiltration in an experimental colitis model (Nowacki et al., 2016), peptide 5A exposure did not influence the quantity of F4/80$^+$ phagocytes in the CC of cuprizone-fed animals (Figures S1L and S1M). Altogether, these findings show that the reparative impact of peptide 5A is associated with increased clearance of myelin and an elevated cellular lipid load.

So far, we have established that ApoA-I promotes remyelination and, in parallel, increases cellular lipid droplet load in the cerebellar brain slice and cuprizone models. Given the importance of macrophages and microglia in the clearance of myelin debris and remyelination (Bogie et al., 2020; Grajchen et al., 2020), we next assessed whether depletion of these phagocytes using clodronate liposomes counteracts the protective impact of peptide 5A on these processes in the cerebellar brain slice model (experimental design in Figure S2A). The efficacy of phagocyte depletion was confirmed by immunohistochemical F4/80 staining of brain slices treated with empty control liposomes and clodronate liposomes (Figures S2B and S2C). Of interest, the absence of F4/80$^+$ phagocytes counteracted the protective effects of peptide 5A on remyelination and degenerated myelin abundance (Figures 3A–3C), indicating that peptide 5A promotes remyelination in a phagocyte-dependent manner.

Peptide 5A promotes lipid droplet load in macrophages and microglia *in vitro*

To determine the effects of peptide 5A on the metabolic and inflammatory properties of phagocytes *in vitro*, primary murine bone marrow-derived macrophages (BMDMs) and microglia were treated with peptide 5A. Like in the brain slice and cuprizone models, we observed that peptide 5A increased cellular lipid droplet formation in a time-dependent fashion in macrophages and microglia, evidenced by an increased BODIPY load and fluorescence intensity (Figures 4A–4C). Consistent with these findings, peptide 5A increased cellular ORO load and granularity in BMDM and microglia cultures (Figures 4A, 4D, and 4E). Despite increasing lipid droplet load, no increase in cell size was observed upon peptide 5A exposure (Figure S3A). As the lipid droplet load decreased when BMDMs were cultured in an fetal calf serum (FCS)-depleted environment, FCS is likely the primary source of lipids used for lipid droplet formation in these cultures (Figure S3B). Given that phagocytes containing myelin degradation products are abundantly present during demyelination and remyelination (Bogie et al., 2020), we extended our analysis to myelin-phagocytosing phagocytes. Similar to untreated cultures, BMDMs and microglia exposed to myelin demonstrated increased lipid droplet levels upon exposure to peptide 5A (Figures 4F–4H). By using pharmacological inhibitors of fatty acid and cholesterol synthesis, we further showed that increased lipid droplet formation did not rely on enhanced *de novo* lipid synthesis (Figure S3C). Of note, despite increasing lipid droplet load, peptide 5A promoted cellular efflux from myelin-loaded phagocytes of cholesterol, which is a major component of lipid droplets in foamy phagocytes (Thiam et al., 2013). The impact of peptide 5A on cholesterol efflux was less pronounced in microglia compared with macrophages (Figure 4I). Collectively, these findings show that peptide 5A promotes phagocyte lipid droplet load while increasing cholesterol efflux.

Given that peptide 5A is reported to reduce inflammation in *in vitro* and *in vivo* models of atherosclerosis (Tabet et al., 2010), we next investigated whether peptide 5A could polarize phagocytes toward an antiinflammatory and reparative phenotype. In our hands, peptide 5A exposure did not lead to notable changes in the expression of inflammatory (i.e., *Il6*, *Il1b*, and *Tnfa*) or neurotrophic mediators (i.e., *Cntf*, *Igf1*, *Ngf*, and *Tgfb*) in activated control or myelin-loaded BMDMs and microglia, except for increased *Nos2* and *Il1b* expression in untreated macrophages and microglia, respectively, and decreased *Tnfa* expression in untreated microglia (Figures S3D–S3K). Accordingly, we did not detect any alterations in the expression of these cytokines and neurotrophic mediators in the CC of peptide 5A-treated animals in the cuprizone model (Figures S3L–S3M). Consistent with these findings, by using experimental autoimmune encephalomyelitis (EAE) as an *in vivo* model for CNS inflammation, we found that peptide 5A only marginally improved disease severity (Figure S3N). These findings provide evidence that the pro-regenerative impact of peptide 5A in the cerebellar brain slice and cuprizone models does not rely on changes in the inflammatory and reparative phenotype of phagocytes.

Peptide 5A stimulates lipid uptake in an ABCA1-dependent manner

The cellular lipid droplet pool and composition are dynamically regulated by changes in lipid efflux, synthesis, and uptake (Hasbargen et al., 2020; Vazquez et al., 2020). With respect to efflux, our findings indicate that peptide 5A promotes cellular disposal

(C and D) Analysis of the g ratio (the ratio of the inner axonal diameter to the total outer diameter) (C) and percentage myelinated axons (D) in CC from vehicle- and peptide 5A-treated mice after 6w and 6w+1 (n = 3–5 animals; for each animal 212–400 axons were analyzed).
(E) mRNA expression of *Mbp* and *Plp* in the CC from vehicle- and peptide 5A-treated mice after 6w and 6w+1 (n = 6–7 animals).
(F) Representative images of immunofluorescence PLIN2/F4/80 (scale bar, 20 μm) and degenerated MBP (dMBP) staining (scale bar, 200 μm) of the CC from vehicle- and peptide 5A-treated mice after cuprizone-induced demyelination (6w) and remyelination (6w+1).
(G and H) Quantification of the percentage of PLIN2$^+$ F4/80$^+$ cells/F4/80$^+$ cells (G), and dMBP$^+$ area of the CC (H) from vehicle- and peptide 5A-treated mice after 6w and 6w+1 (n = 4–6 animals). Data are represented as the mean ± SEM; *p < 0.05; **p < 0.01; ***p > 0.001; ****p < 0.0001. See also Figure S1.

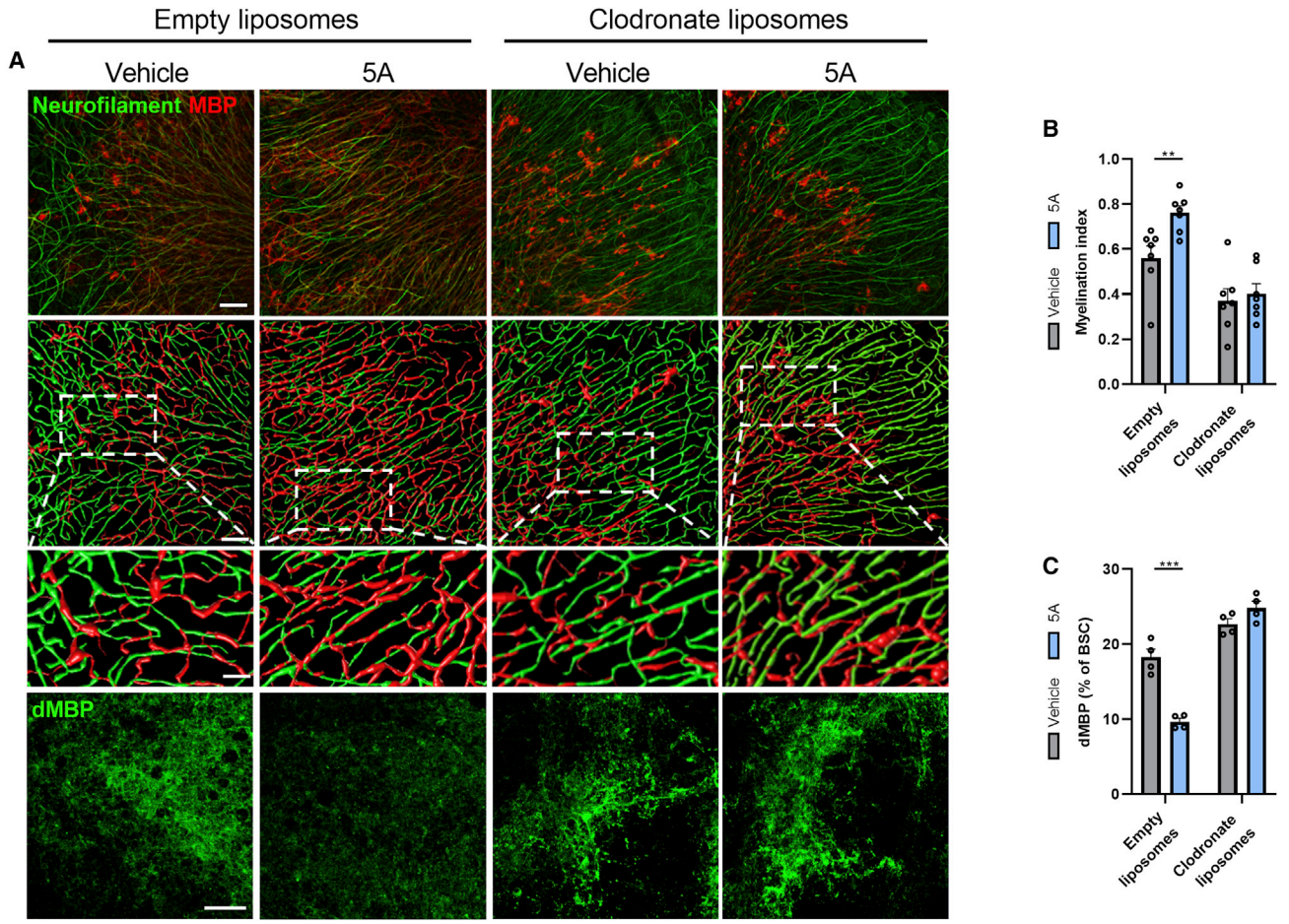

Figure 3. Peptide 5A improves remyelination *ex vivo* in a phagocyte-dependent manner

(A) Representative images (row 1) and three-dimensional reconstruction (rows 2–3) of immunofluorescence myelin (MBP) and neurofilament staining and of degenerated MBP (dMBP) staining of cerebellar brain slices stimulated with empty liposomes or clodronate liposomes (0.5 mg/mL) and treated with vehicle or peptide 5A (50 μg/mL). Scale bars, 50 μm (overview); 20 μm (insets).

(B) Quantification of MBP^+ NF^+ axons out of total NF^+ axons in cerebellar brain slices treated with empty or clodronate liposomes and vehicle or peptide 5A (n = 7 slices).

(C) Quantification of the $dMBP^+$ area of empty or clodronate liposomes and vehicle- or peptide 5A-treated cerebellar brain slice cultures (n = 4 slices). Results are pooled from three biological replicates. Data are represented as the mean ± SEM; $^{**}p < 0.01$; $^{***}p < 0.001$. See also Figure S2.

of cholesterol (Figure 4I), which in its esterified form constitutes one of the main lipid esters in the core of lipid droplets (Thiam et al., 2013). Hence, the peptide 5A-induced increase in lipid droplets is not due to compromised lipid efflux. Likewise, we show that peptide 5A exposure did not lead to notable changes in the activity and expression of lipases, hydrolases, and acyltransferases involved in the catabolism and anabolism of lipid droplet-associated cholesterol ester (CE) and acylglycerides (Figures 5A and S3C). In addition, peptide 5A did not affect the autophagy machinery (Figures S3O–S3Q), which is essential for lipid droplet breakdown (Haidar et al., 2021). These findings suggest that changes in the cellular metabolism of CE and triglycerides (TG) do no account for the peptide 5A-induced increase in lipid droplets. Interestingly, the expression of the cholesterol-sensing nuclear receptors *Lxra* and *Lxrb* was decreased upon prolonged exposure to peptide 5A (Figure 5B). To investigate whether increased lipid uptake underlies the observed increase in lipid droplets after peptide 5A treatment, we assessed the phagocytic capacity of BMDMs and microglia. Phagocytosis experiments demonstrated increased uptake of fluorescently labeled myelin and latex beads by BMDMs and microglia exposed to peptide 5A (Figures 5C–5F, S3O and S3R). These findings indicate that changes in the cellular lipid droplet pool upon peptide 5A exposure likely rely on an increased capacity to internalize extracellular lipid-containing ligands.

The binding of ApoA-I to the cholesterol efflux receptor ABCA1 is well known to promote efflux of cellular cholesterol and phospholipids (Stamatikos et al., 2019; Vaughan and Oram, 2003). Therefore, we next determined whether the interaction between ABCA1 and ApoA-I was also necessary for the uptake of myelin and latex beads. By using *Abca1*-deficient murine BMDMs, we showed that peptide 5A loses its ability to increase the uptake of myelin and latex beads in the absence of ABCA1 (Figure 5C and 5E). Accordingly, lack of ABCA1 nullified the observed

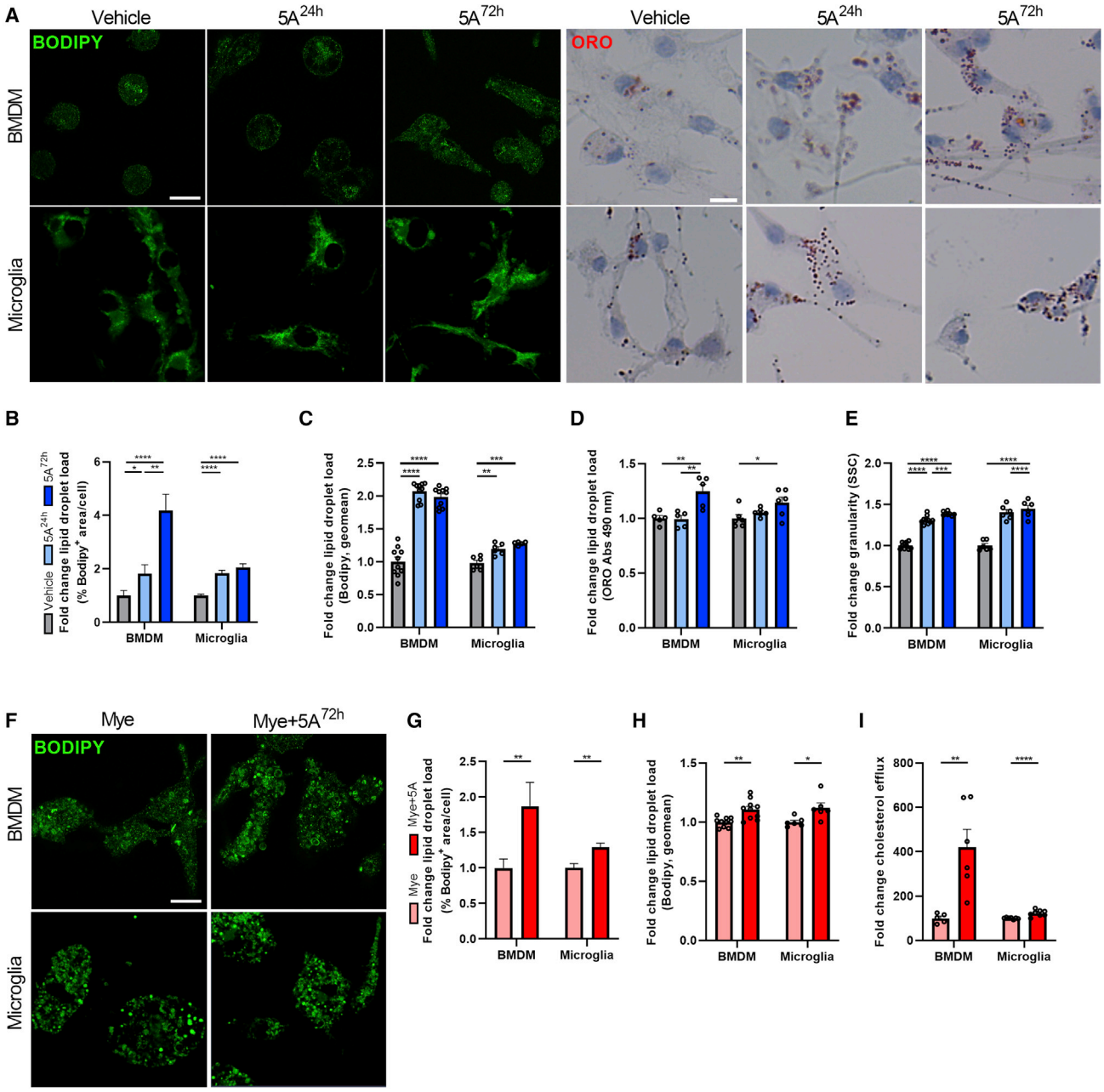

Figure 4. Peptide 5A promotes lipid droplet load in macrophages and microglia *in vitro*

(A) Representative images of BODIPY (left) and oil red O (ORO; right) staining of bone marrow-derived macrophages (BMDMs; top) and microglia (bottom) treated with vehicle or peptide 5A (10 μg/mL) for 24 or 72 h. Scale bars, 10 μm (left) and 20 μm (right).

(B) Quantification of percentage BODIPY$^+$ area per BMDM and microglia treated with vehicle (n = 61 cells [BMDMs] and 52 cells [microglia]) or peptide 5A for 24 h (n = 67 cells [BMDMs] and 47 cells [microglia]) or 72 h (n = 102 cells [BMDMs] and 48 cells [microglia]).

(C) Mean fluorescence intensity of BODIPY in BMDMs (n = 10) and microglia (n = 6) treated with vehicle or peptide 5A for 24 or 72 h.

(D) Quantification of ORO load in BMDMs (n = 5) and microglia (n = 6) treated with peptide 5A for 24 or 72 h.

(E) Granularity measured as side scatter (SSC) by means of flow cytometry in BMDMs (n = 8–10) and microglia (n = 6) treated with vehicle or peptide 5A for 24 or 72 h.

(F) Representative images of BODIPY staining of BMDMs and microglia treated with myelin (100 μg/mL) with or without peptide 5A for 72 h. Scale bar, 10 μm.

(G) Quantification of percentage BODIPY$^+$ area per BMDM and microglia treated with myelin with (n = 44 cells [BMDMs] and 45 cells [microglia]) or without (n = 57 cells [BMDMs] and 28 cells [microglia]) peptide 5A for 72 h.

(H) Mean fluorescence intensity of BODIPY in BMDMs (n = 10) and microglia (n = 6) treated with myelin with or without peptide 5A for 72 h.

(I) Relative capacity to efflux cholesterol of BMDMs (n = 5–6) and microglia (n = 8) treated with myelin for 72 h and peptide 5A for 4 h (50 μg/mL). Results are pooled from two (D, I) or three (A–C, E–H) biological replicates. Data are represented as the mean ± SEM; *p < 0.05; **p < 0.01; ***p < 0.001; ****p < 0.0001.

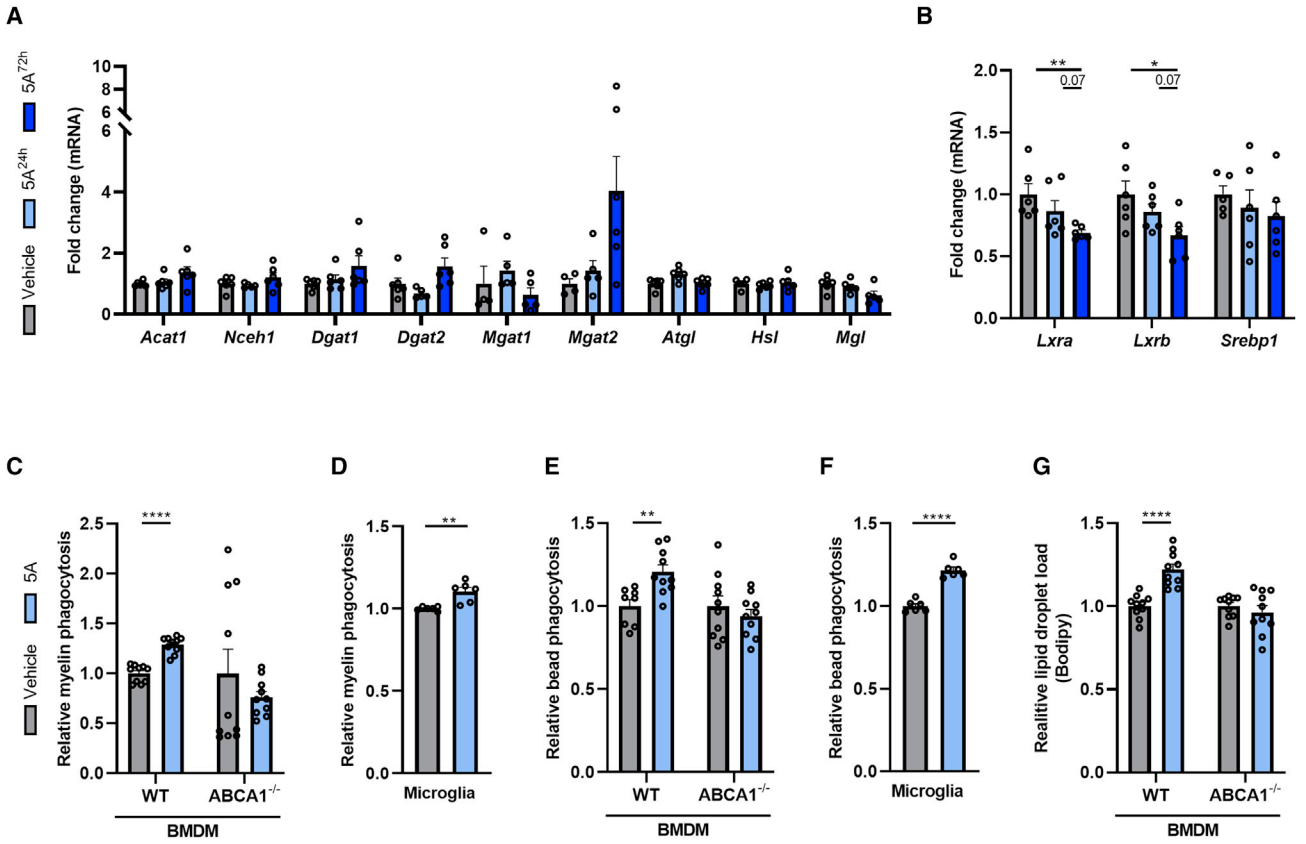

Figure 5. Peptide 5A enhances macrophage and microglia phagocytosis in an ABCA1-dependent manner

(A) mRNA expression of genes involved in the anabolism and catabolism of cholesterol and acylglycerides in bone marrow-derived macrophages (BMDMs) treated with vehicle or peptide 5A (10 μg/mL) for 24 and 72 h (n = 4–6).

(B) mRNA expression of genes involved in the synthesis of cholesterol in BMDMs treated with vehicle or peptide 5A for 24 and 72 h (n = 5).

(C–F) Internalization of DiI-labeled myelin (C and D) and fluorescently labeled beads (E and F) by wild-type (WT) and ABCA1$^{-/-}$ BMDMs (C and E; n = 10) and WT microglia (D and F; n = 6) treated with vehicle or peptide 5A for 24 h. Data are depicted as the mean fluorescence intensity as defined by flow cytometry.

(G) Mean fluorescence intensity of BODIPY in WT and ABCA1$^{-/-}$ BMDMs treated with vehicle or peptide 5A for 24 h (n = 10). Results are pooled from two (A and B) or three (C–G) biological replicates. Data are represented as the mean ± SEM; *p < 0.05; **p < 0.01; ****p < 0.0001. See also Figure S3.

increase in lipid droplets in BMDMs exposed to peptide 5A, as measured by BODIPY fluorescence intensity (Figure 5G). Altogether, these data indicate that peptide 5A increases the phagocytic capacity of murine macrophages in an ABCA1-dependent manner and suggest that increased uptake of extracellular lipids and lipid-containing complexes underlies the accumulation of lipid droplets upon peptide 5A treatment.

Peptide 5A increases cellular triglyceride and phospholipid levels but decreases the cholesteryl ester pool

To assess changes in the cellular lipidome and identify lipid species preferentially taken up by phagocytes after peptide 5A exposure, liquid chromatography electrospray ionization tandem mass spectrometry (LC-ESI-MS/MS) was performed. In line with increased cholesterol efflux (Figure 4I), BMDMs exposed to peptide 5A demonstrated reduced intracellular levels of CE (Figure 6A). Decreased levels of CE, as well as free and total cholesterol, were confirmed in BMDMs and microglia using the Amplex red assay (Figures 6B and 6C) and may provide a molecular rationale for the reduced expression of the cholesterol-sensing nuclear receptors *Lxrα* and *Lxrβ* following peptide 5A exposure (Figure 5D). Interestingly, in contrast to cholesterol, peptide 5A markedly increased the level of TG in BMDMs. Given that lipid droplets consist predominantly of neutral lipids, the observed changes in CE and TG are likely to reflect changes in lipid droplet composition. In addition to increasing TG levels, peptide 5A increased the abundance of several major phospholipid classes typically found in the monolayer surrounding lipids droplets (Thiam et al., 2013), i.e., phosphatidylcholine (PC), phosphatidylethanolamine (PE), and phosphatidylinositol (PI) (Figure 6A). In-depth analysis further demonstrated that the relative abundance of C20 and/or C22 fatty acids was increased in the majority of lipid species at the expense of C14-C18 fatty acids (Figure 6D; details of fatty acid composition in Figure S4A). Similar to alterations in the abundance of CE and TG, the increase in phospholipids could not be ascribed to changes in the expression of lipases and acyltransferases involved in their formation and breakdown (Figures S4B and S4C). Specifically, the expression of lipases such as *Pla2g4b*, *Pla2g4c*, *Pla2g2e*, and *Pla2g5* was increased in BMDMs exposed

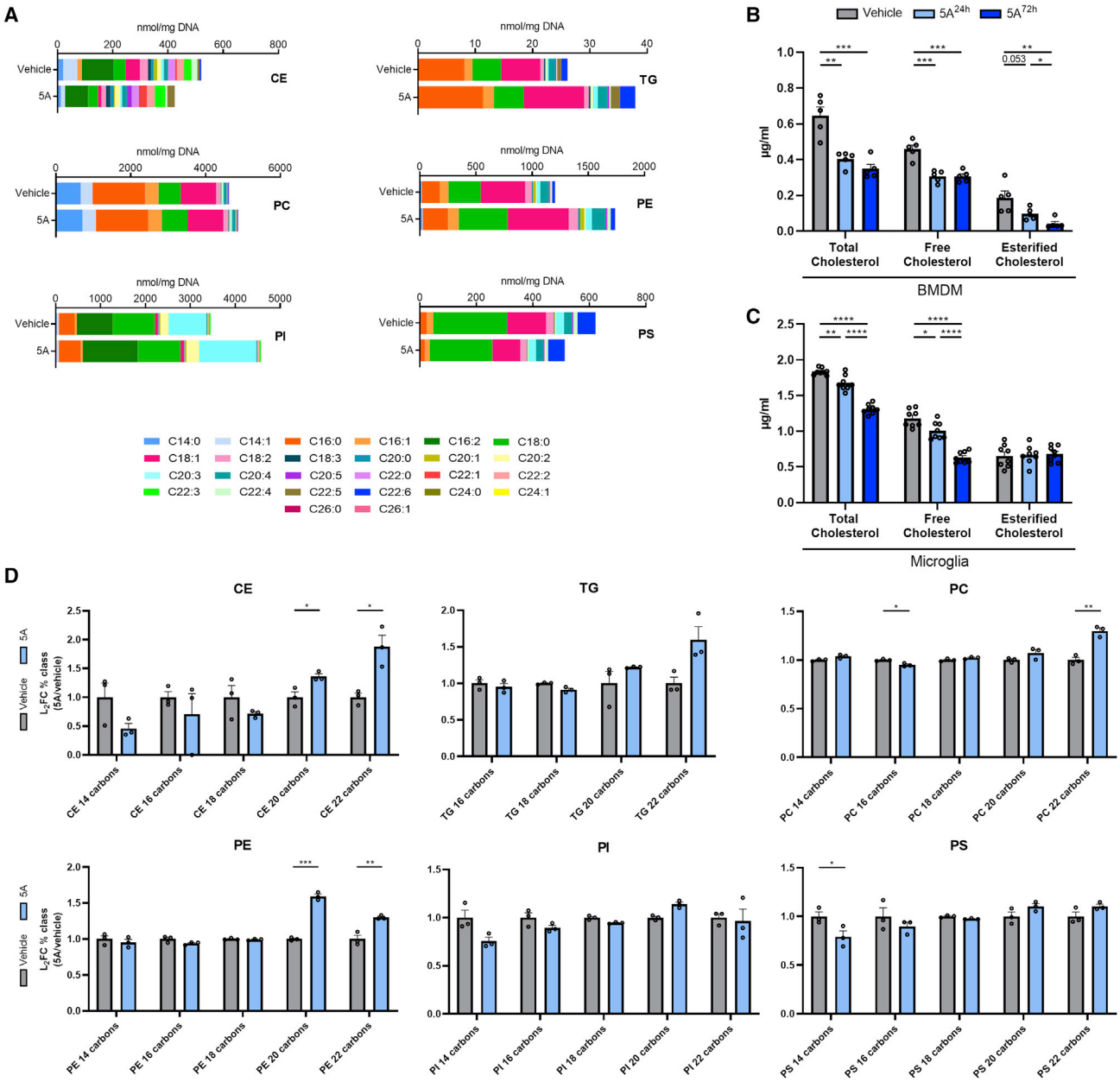

Figure 6. Peptide 5A increases cellular triglyceride and phospholipid levels but decreases cellular cholesteryl ester levels

(A) Liquid chromatography electrospray tandem mass spectrometry (LC-ESI-MS/MS) analysis of bone marrow-derived macrophages (BMDMs) treated with vehicle or peptide 5A (10 µg/mL) for 72 h. Fatty acid composition of cholesterol ester (CE), triglycerides (TG), phosphatidylcholine (PC), phosphatidylethanolamine (PE), phosphatidylinositol (PI), and phosphatidylserine (PS) is shown (n = 3).

(B and C) Quantification of total cholesterol, free cholesterol, and esterified cholesterol in BMDMs (B; n = 5) and microglia (C; n = 8) treated with vehicle or peptide 5A for 24 or 72 h.

(D) Analysis of the fatty acid length classes of CE, TG, PC, PE, PI, and PS of BMDMs treated with vehicle or peptide 5A for 72 h. Data are depicted as log2 fold change (L_2FC) of the percentage of each class compared with vehicle (n = 3). Results are pooled from two (B and C) or three (A and D) biological replicates. Data are represented as the mean ± SEM; *p < 0.05; **p < 0.01; ***p < 0.001; ****p < 0.0001. See also Figure S4.

to peptide 5A, which does not mirror elevated levels of PC, PE, and PI (Figure S4B). Interestingly, peptide 5A markedly increased the expression of acyltransferases such as *Mboat1* and *Lpgat1* (Figure S4C). However, the abundance of long-chain saturated fatty acyl-CoAs such as oleoyl-CoA (C18), which are preferred acyl donors of MBOAT1 and LPGAT1, did not differ between control and peptide 5A-treated macrophages (Figure 6D). This finding suggests that enhanced expression of acyltransferases does not explain changes in the level of PC, PE, and PI upon peptide 5A exposure. Finally, we detected increased sphingomyelin (SM)

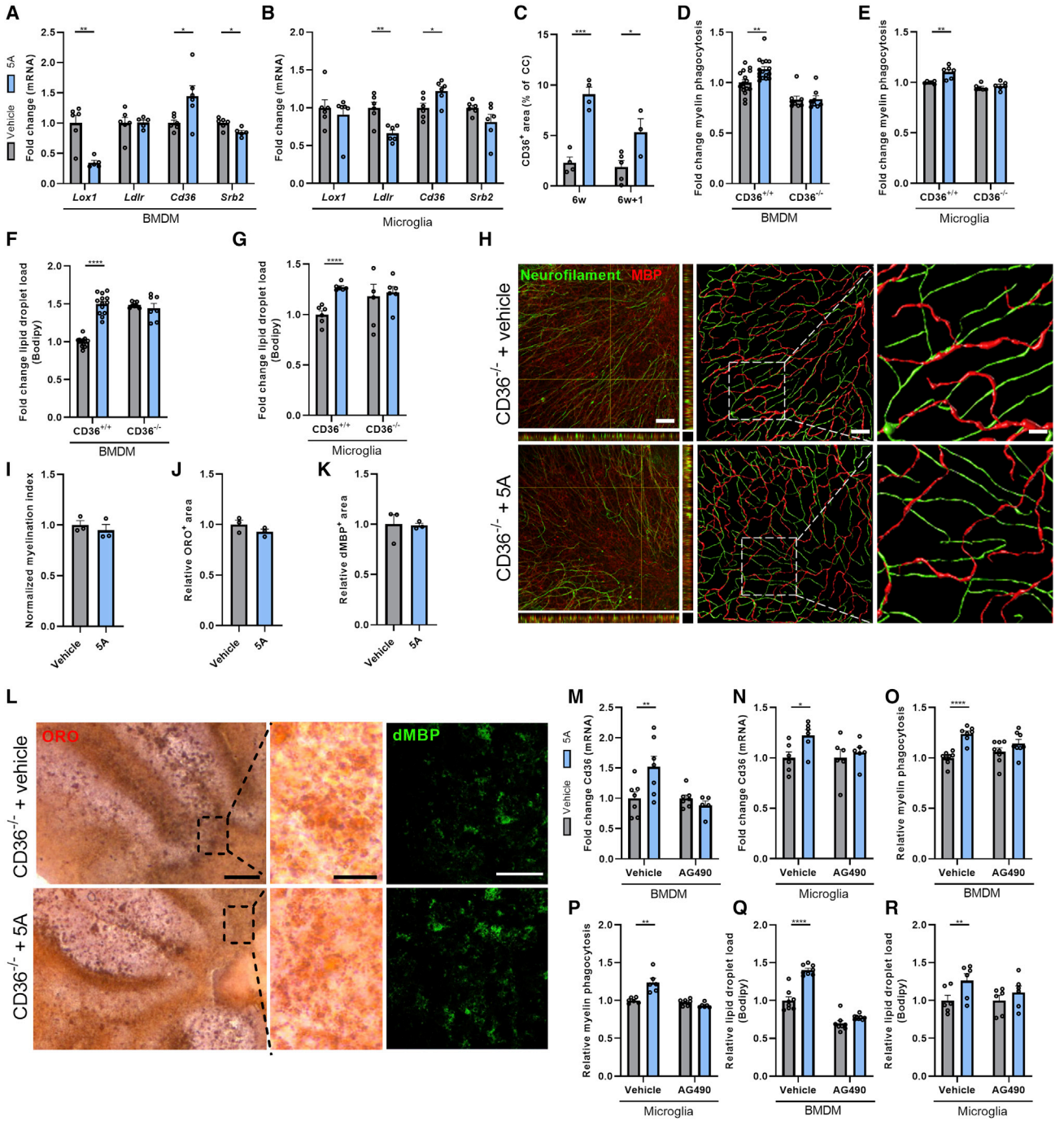

Figure 7. Peptide 5A promotes CD36-mediated lipid uptake in a JAK2/STAT3-dependent manner

(A and B) mRNA expression of scavenger receptors in bone marrow-derived macrophages (BMDMs; A) and microglia (B) treated with vehicle or peptide 5A (10 μg/mL) for 72 h (n = 5–6).

(C) Quantification of the $CD36^+$ area of the corpus callosum from vehicle- and peptide 5A (30 mg/kg)-treated mice after cuprizone-induced demyelination (6w) and remyelination (6w+1) (n = 3–5 animals).

(D and E) Internalization of DiI-myelin by wild-type and $CD36^{-/-}$ BMDMs (D; n = 8–16) and microglia (E; n = 6) treated with vehicle or peptide 5A for 72 h.

(F and G) BODIPY intensity in wild-type and $CD36^{-/-}$ BMDMs (F; n = 5–13) and microglia (G; n = 6) treated with vehicle or peptide 5A for 72 h.

(H and I) Representative images, orthogonal projections (column 1), and three-dimensional reconstruction (columns 2–3, H) of immunofluorescence MBP and neurofilament staining and normalized quantification (I) of MBP^+NF^+ axons/NF^+ axons of $CD36^{-/-}$ cerebellar brain slice cultures treated with vehicle or peptide 5A (50 μg/mL). Scale bars, 50 μm (overview), 20 μm (insets) (n = 3 slices).

(legend continued on next page)

levels in BMDMs treated with peptide 5A (Figure S4D), which probably reflects uptake of SM that is pre-complexed to peptide 5A. In support of this notion, peptide 5A-treated BMDMs demonstrated a relative increase in C14-C18 fatty acid levels in SM, which represent the major fatty acids in peptide 5A-complexed SM (Figure S4E). Altogether, these findings show that peptide 5A changes the cellular lipidome of macrophages, with considerable changes in the levels of lipid droplet-associated neutral lipids such as CE and TG and enrichment of C20 and C22 fatty acids.

Peptide 5A promotes CD36-mediated lipid uptake in a JAK2/STAT3-dependent manner

Our data indicate that peptide 5A increases lipid droplet formation by promoting the uptake of lipid-containing complexes by phagocytes in an ABCA1-dependent manner. Here, we aimed to identify the receptors that drive the increased phagocytic capacity of phagocytes upon peptide 5A exposure. For this purpose, the expression of receptors known to be involved in the uptake of myelin, latex beads, and (C20/C22) fatty acids (and fatty acid-containing complexes), and those regulated by the ABCA1 signaling pathway, was determined in murine BMDMs and microglia (Drover et al., 2008; Grajchen et al., 2018; Zhao et al., 2012). Our findings show that peptide 5A increased the expression of the fatty acid translocase *Cd36* in BMDMs and microglia, but did not induce mRNA levels of *Lox1*, *Ldlr*, or *Srb2* (Figures 7A and 7B). Accordingly, CD36 abundance was increased in the CC of peptide 5A-treated mice in the cuprizone model (Figures 7C and S5A). By using *Cd36*$^{-/-}$ BMDMs and microglia, we further found that peptide 5A was no longer able to promote the uptake of fluorescently labeled myelin and latex beads by BMDMs and microglia in the absence of CD36 (Figures 7D, 7E, S5B, and S5C). Consistent with these changes, CD36 deficiency counteracted the observed increase in lipid droplets upon peptide 5A exposure in BMDM and microglia cultures (Figures 7F and 7G). *Cd36* deficiency did not have an impact on enhanced cholesterol efflux upon exposure to peptide 5A (Figures S5D and S5E). Consistent with *in vitro* findings, the absence of CD36 counteracted the observed pro-regenerative and metabolic impact of peptide 5A in the brain slice model (Figures 1 and 7H–7L), as evidenced by an inability of peptide 5A to enhance remyelination (Figures 7H and 7I), increase cellular lipid droplet load (Figures 7J and 7L), or clear damaged myelin debris (Figures 7K and 7L). These findings show that peptide 5A stimulates the uptake of myelin and latex beads in a CD36-dependent manner, and strongly suggest that peptide 5A promotes remyelination through CD36-mediated clearance of myelin debris.

Previous studies showed that the JAK2/STAT3 signaling cascade is activated upon binding of ApoA-I to ABCA1 (Tang et al., 2004, 2009), and that its activation induces CD36 on a transcriptional level (Bhattacharjee et al., 2013). By using AG490, a JAK2/STAT3 inhibitor, we found that peptide 5A enhanced *Cd36* expression in phagocytes via the JAK2/STAT3 signaling pathway (Figures 7M and 7N). Consistent with these findings, AG490 counteracted the peptide 5A-mediated increased uptake of myelin and latex beads (Figures 7O, 7P, S5F, and S5G), and reduced lipid droplet load in BMDMs and microglia (Figures 7Q and 7R). These results indicate that peptide 5A controls *Cd36* expression and activity through the JAK2/STAT3 signaling cascade. Collectively, findings from this study demonstrate that peptide 5A promotes CD36-mediated myelin debris clearance in an ABCA1/JAK2/STAT3-dependent manner, thereby inducing a repair-permissive environment.

DISCUSSION

Recently, we and others demonstrated that an impaired ability to dispose of internalized myelin-derived cholesterol via the cholesterol efflux transporter ABCA1 induces a phagocyte phenotype that suppresses CNS repair (Bogie et al., 2020). In this study, we report that the ApoA-I mimetic peptide 5A, a molecule well known to promote ABCA1 stabilization and activity, markedly enhances remyelination in the cerebellar brain slice and cuprizone models. Mechanistically, peptide 5A reduced intracellular phagocyte cholesterol load and enhanced clearance of myelin debris, which are both processes predicted to promote remyelination (Bogie et al., 2020; Cantuti-Castelvetri et al., 2018; Lampron et al., 2015; Marschallinger et al., 2020). Improved clearance of myelin debris was attributed to increased expression of the fatty acid translocase CD36 in phagocytes, which we found to be transcriptionally regulated via the ABCA1-JAK2-STAT3 pathway. Collectively, our findings indicate that peptide 5A is a promising therapeutic compound to enhance remyelination in demyelinating pathologies.

In this study, we provide evidence that the ApoA-I mimetic peptide 5A promotes remyelination *ex vivo* and *in vivo*. In line with these findings, previous studies demonstrated that ApoA-I is essential for peripheral tissue repair, and that HDL, ApoA-I, and ApoE mimetic peptides cross the blood-brain barrier, accumulate in the CNS, and affect brain pathology in experimental disease models (Button et al., 2019; Gu et al., 2013; Lewis et al., 2010; Liu et al., 2017; Peterson et al., 2007; Rosenbaum et al., 2015; Swaminathan et al., 2020). In particular, ApoA-I overexpression or mimetic peptides were found to promote vascular repair in models of atherosclerosis and diabetes, and prevent cognitive deficits and cerebral amyloid angiopathy in an Alzheimer's disease model (Lewis et al., 2010; Liu et al., 2017; Peterson et al., 2007; Rosenbaum et al., 2015). Furthermore, the ApoE-mimetic peptide COG112 was demonstrated to diminish

(J–L) Quantification of the degenerated MBP^{+} (dMBP^{+}) (J) and ORO^{+} (K) area and representative images (L) of immunofluorescence dMBP staining (scale bar, 50 μm), and oil red O (ORO) staining (scale bars, 100 μm [overview]; 25 μm [insets]) of CD36$^{-/-}$ cerebellar brain slice cultures treated with vehicle or peptide 5A (n = 3 slices).
(M and N) *Cd36* expression of BMDMs (M; n = 5–7) and microglia (N; n = 6) treated with vehicle, peptide 5A, and/or the Jak2/Stat3 inhibitor AG490 (25 μM) for 72 h.
(O and P) Internalization of DiI-myelin by BMDMs (O; n = 8) and microglia (P; n = 6) treated with vehicle, peptide 5A, and/or the Jak2/Stat3 inhibitor AG490 for 72 h.
(Q and R) BODIPY intensity in BMDMs (Q; n = 8) and microglia (R; n = 6) treated with vehicle or peptide 5A for 72 h, with or without the JAK2/STAT3 inhibitor AG490. Results are pooled from two (A and B, D–G [CD36$^{-/-}$], I–K) or three (D–G [vehicle], M–R) biological replicates. Data are represented as the mean ± SEM; *p < 0.05; **p < 0.01; ***p < 0.001; ****p < 0.0001. See also Figure S5.

demyelination and promote remyelination in a lysolecithin-induced spinal cord demyelination model (Gu et al., 2013). We further show that enhanced remyelination in peptide 5A-exposed cuprizone animals and brain slice cultures is associated with a reduced presence of degenerated myelin and increased lipid droplet load in F4/80$^+$ phagocytes. Importantly, by using clodronate liposomes, we find that the pro-regenerative impact of peptide 5A in brain slice cultures relies on changes in phagocyte physiology. These findings argue that the reparative impact of peptide 5A relies on changes in phagocyte physiology. However, given that ApoA-I promotes nascent HDL formation and can have an impact on a variety of cells (Chinetti et al., 2001; Karten et al., 2006; Sengupta et al., 2017), we cannot exclude the impact of changes in lipoproteins and other cells on remyelination in the cuprizone model.

By using *in vitro* models that mimic the formation of foamy macrophages and microglia in the CNS, we found that peptide 5A promotes cholesterol efflux and reduces the intracellular free and esterified cholesterol load of myelin-containing phagocytes. Consistent with these findings, peptide 5A, as well as other ApoA-I mimetic peptides, is reported to promote ABCA1-mediated cholesterol efflux (Amar et al., 2010; Gou et al., 2020; Meriwether et al., 2016; Navab et al., 2004; Schwendeman et al., 2015; Sherman et al., 2010; Sviridov et al., 2013). However, while excessive accumulation of cholesterol drives foamy phagocytes toward an inflammatory disease-promoting phenotype characterized by an increased expression of *Tnfa*, *Il1b*, *Il6*, and *Nos2* (Bogie et al., 2020; Cantuti-Castelvetri et al., 2018), peptide 5A did not reduce the expression of these repair-suppressive mediators, nor did it increase the expression of neurotrophic mediators in myelin-containing macrophages and microglia (Cantuti-Castelvetri et al., 2018; Karamita et al., 2017; Lan et al., 2018; Makinodan et al., 2016; Vela et al., 2002). In line with these findings, peptide 5A did not change the expression of these markers in the CC of cuprizone animals, and did not reduce disease severity in the EAE model, an experimental model that mimics autoimmune-associated neuroinflammation. These findings suggest that the pro-regenerative impact of peptide 5A is autonomous of changes in the neuroinflammatory environment and that its therapeutic potential is limited to promoting remyelination.

Despite enhancing cholesterol efflux, our data indicate that peptide 5A markedly increases the lipid droplet load in phagocytes *in vitro* and *in vivo*. Moreover, our findings demonstrate that peptide 5A decreases and increases lipid droplet-associated CE and TG content, respectively. While the decrease in cellular CE levels might merely be a consequence of enhanced cholesterol efflux, the quantitative increase in TG cannot be explained by changes in lipid efflux. Instead, based on our findings, we postulate that peptide 5A increases the uptake of fatty acid-containing ligands from the microenvironment and promotes their subsequent storage in lipid droplets. Despite the increased lipid load in phagocytes, we show that peptide 5A promotes remyelination *ex vivo* and *in vivo*. This finding suggests that the lipid droplet composition, rather than quantity, may serve as a predictive marker for identifying the reparative properties of foamy phagocytes in the CNS (Marschallinger et al., 2020). Accordingly, emerging evidence indicates the existence of diverse multifunctional lipid droplet populations that can be discriminated based on their distinct lipid compositions (Thiam and Beller, 2017). This recently recognized diversity is anticipated to have a major impact on cellular function (Bailey et al., 2015; D'Ambrosio et al., 2011; Liu et al., 2015), and with respect to our findings, raises the question whether enrichment of TG and C20/C22 fatty acids characterizes the formation of benign lipid droplets in phagocytes. Of interest, lipid droplet-associated TG are reported to alter the physical state of CE, enabling efficient hydrolysis and efflux of cholesterol (Lada et al., 2002). Hence, it is tempting to speculate that the observed increase in lipid droplet TG upon peptide 5A exposure ensues to catalyze cholesterol efflux. However, more research is warranted to unravel the molecular mechanisms that drive changes in lipid droplet composition upon peptide 5A exposure, and to what extent these changes influence macrophage and microglia physiology.

We show that peptide 5A promotes the expression of the fatty acid translocase CD36 and that increased CD36 expression underlies enhanced uptake of myelin debris by phagocytes upon peptide 5A exposure *in vitro*. These findings substantiate the importance of CD36 in the clearance of myelin debris (Grajchen et al., 2020) and provide a molecular rationale for reduced levels of degenerated myelin debris and enhanced remyelination in peptide 5A-treated cuprizone animals. However, despite increased CD36 expression and PLIN2 abundance in F4/80$^+$ phagocytes upon peptide 5A exposure, further research is warranted to verify peptide 5A-driven CD36-mediated myelin debris clearance *in vivo*. The observed increase in TG, PC, PE, and PI in our lipidomic analysis further confirms the essential role of CD36 in driving the uptake of fatty acid-containing ligands (Chrast et al., 2011; Coburn et al., 2000; Grajchen et al., 2020; Hames et al., 2014; Pohl et al., 2005). Finally, we provide evidence that peptide 5A controls CD36 expression through the JAK2/STAT3 signaling pathway. Accordingly, previous studies found that the JAK2/STAT3 signaling cascade is activated upon binding of ApoA-I to ABCA1 (Tang et al., 2004, 2009), and that JAK2/STAT3 controls CD36 on a transcriptional level (Bhattacharjee et al., 2013). It is worth mentioning that activation of the JAK2/STAT3 signaling pathways promotes oligodendrogenesis and repair in a spinal cord injury model as well (Hesp et al., 2015). Hence, aside from promoting myelin clearance, peptide 5A may favor remyelination by stimulating oligodendrogenesis.

Previous studies showed that HDL and ApoA-I mimetic peptides efficiently cross the blood-brain barrier, accumulate in the CNS, and affect brain pathology in experimental disease models (Button et al., 2019; Swaminathan et al., 2020). Moreover, Swaminathan et al. demonstrated that brain permeability to the ApoA-I mimetic peptide 4F is approximately 1,000-fold greater than that to endogenous ApoA-I in mice (Swaminathan et al., 2020). Based on these studies, we anticipate that peptide 5A is likely to accumulate in appreciable amounts in the CNS of cuprizone-fed animals. Moreover, cuprizone-fed mice show increased blood-brain barrier permeability and extensive infiltration of blood-derived macrophages in the CNS (Berghoff et al., 2017; McMahon et al., 2002; Shelestak et al., 2020), further promoting CNS bioavailability of peptide 5A. In future studies, tracking experiments using radioisotope-labeled peptide 5A could unravel the CNS bioavailability of peptide 5A in healthy

and cuprizone mice. Such experiments would also allow for spatiotemporal tracking of peptide 5A. Of interest, our lipidomics analysis already suggests that peptide 5A, which is pre-complexed with SM, is internalized by macrophages and microglia, as SM levels increase upon peptide 5A exposure. However, as it is a substrate for the generation of discoid HDL precursors, we also anticipate that peptide 5A exists extracellularly in the form of cholesterol-rich nascent HDL particles in the CNS parenchyma. With respect to this, horizontal lipid flux is increasingly being acknowledged as essential in supplying OPCs with the necessary lipids for myelin formation (Camargo et al., 2017).

In summary, our findings indicate that the ApoA-I mimetic peptide 5A enhances remyelination by promoting both ABCA1-mediated cholesterol efflux and CD36-mediated clearance of myelin debris by macrophages and microglia. Taken together, our findings demonstrate that peptide 5A potentially has broad implications for therapeutic strategies aimed at promoting CNS repair.

Limitations of the study

In this study, we applied primary mouse cell cultures, cerebellar brain slices, and the cuprizone model to study the impact of peptide 5A on remyelination in demyelinating pathologies. While these experimental models represent the gold standard for studying CNS regeneration, remyelination in humans may not precisely mirror pathological and regenerative changes in these models. Similarly, few studies indicate that mice exhibit significant differences in lipid metabolism compared with humans. Hence, care should be taken to translate our findings to patients. Moreover, while our findings strongly suggest that peptide 5A improves remyelination in a phagocyte-dependent manner in the cerebellar brain slice model, we cannot exclude that peptide 5A enhances remyelination in the cuprizone model by modulating the regenerative properties of other cells as well.

STAR★METHODS

Detailed methods are provided in the online version of this paper and include the following:

- KEY RESOURCES TABLE
- RESOURCE AVAILABILITY
  - Lead contact
  - Materials availability
  - Data and code availability
- EXPERIMENTAL MODEL AND SUBJECT DETAILS
  - Animals
  - Cuprizone-induced acute demyelination *in vivo* model
  - Experimental autoimmune encephalomyelitis
  - Cerebellar brain slice cultures
  - Cell isolation and culture
  - Myelin isolation
- METHOD DETAILS
  - Antibodies and chemical reagents
  - Peptide 5A
  - Myelin phagocytosis
  - Quantitative PCR
  - Immunofluorescence
  - Oil Red O staining
  - Flow cytometry
  - Transmission electron microscopy
  - Cholesterol measurements
  - LC-ESI-MS/MS
- QUANTIFICATION AND STATISTICAL ANALYSIS
  - Statistical analysis

SUPPLEMENTAL INFORMATION

Supplemental information can be found online at https://doi.org/10.1016/j.celrep.2022.111591.

ACKNOWLEDGMENTS

We thank M.P. Tulleners for excellent technical assistance. The work was financially supported by the Research Foundation of Flanders (FWO Vlaanderen; 1S15519N, G099618FWO, and 12J9119N) and the Interreg V-A EMR program (EURLIPIDS, EMR23). The funding agencies had no role in the design, analysis, or writing of the article.

AUTHOR CONTRIBUTIONS

S.V., J.J.A.H., and J.F.J.B. conceived the experiments. S.V., W.J., T.D., M.L., E.G., F.M., J.G., P.G., and J.D. performed the experiments. S.V., W.J., T.D., M.L., E.G., F.M., J.G., J.D., M.H., and J.F.J.B. analyzed the data. S.V., W.J., T.D., M.L., E.G., F.M., J.V.S., M.T.M., A.T.R., M.H., J.J.A.H., and J.F.J.B. discussed the results. P.G., I.L., J.D., J.V.S., M.T.M., and A.T.R. contributed reagents, materials, and analysis tools. S.V., M.H., J.J.A.H., and J.F.J.B. wrote the manuscript. S.V., W.J., T.D., M.L., E.G., F.M., J.G., P.G., I.L., J.D., J.V.S., M.T.M., A.T.R., M.H., J.J.A.H., and J.F.J.B. revised the manuscript.

DECLARATION OF INTERESTS

The authors declare no competing interests.

INCLUSION AND DIVERSITY

We support inclusive, diverse, and equitable conduct of research.

Received: April 21, 2022
Revised: September 9, 2022
Accepted: October 11, 2022
Published: November 8, 2022

REFERENCES

Amar, M.J.A., D'Souza, W., Turner, S., Demosky, S., Sviridov, D., Stonik, J., Luchoomun, J., Voogt, J., Hellerstein, M., Sviridov, D., and Remaley, A.T. (2010). 5A apolipoprotein mimetic peptide promotes cholesterol efflux and reduces atherosclerosis in mice. J. Pharmacol. Exp. Ther. *334*, 634–641.

Bailey, A.P., Koster, G., Guillermier, C., Hirst, E.M.A., MacRae, J.I., Lechene, C.P., Postle, A.D., and Gould, A.P. (2015). Antioxidant role for lipid droplets in a stem cell niche of Drosophila. Cell *163*, 340–353.

Berghoff, S.A., Düking, T., Spieth, L., Winchenbach, J., Stumpf, S.K., Gerndt, N., Kusch, K., Ruhwedel, T., Möbius, W., and Saher, G. (2017). Blood-brain barrier hyperpermeability precedes demyelination in the cuprizone model. Acta Neuropathol. Commun. *5*, 94.

Berghoff, S.A., Spieth, L., Sun, T., Hosang, L., Schlaphoff, L., Depp, C., Düking, T., Winchenbach, J., Neuber, J., Ewers, D., et al. (2021). Microglia facilitate repair of demyelinated lesions via post-squalene sterol synthesis. Nat. Neurosci. *24*, 47–60.

Bhattacharjee, A., Shukla, M., Yakubenko, V.P., Mulya, A., Kundu, S., and Cathcart, M.K. (2013). IL-4 and IL-13 employ discrete signaling pathways for

target gene expression in alternatively activated monocytes/macrophages. Free Radic. Biol. Med. *54*, 1–16.

Bogie, J.F.J., Jorissen, W., Mailleux, J., Nijland, P.G., Zelcer, N., Vanmierlo, T., Van Horssen, J., Stinissen, P., Hellings, N., and Hendriks, J.J.A. (2013). Myelin alters the inflammatory phenotype of macrophages by activating PPARs. Acta Neuropathol. Commun. *1*, 43.

Bogie, J.F.J., Mailleux, J., Wouters, E., Jorissen, W., Grajchen, E., Vanmol, J., Wouters, K., Hellings, N., Horssen, J.v., Vanmierlo, T., and Hendriks, J.J.A. (2017). Scavenger receptor collectin placenta 1 is a novel receptor involved in the uptake of myelin by phagocytes. Sci. Rep. *7*, 46925.

Bogie, J.F.J., Timmermans, S., Huynh-Thu, V.A., Irrthum, A., Smeets, H.J.M., Gustafsson, J.Å., Steffensen, K.R., Mulder, M., Stinissen, P., Hellings, N., and Hendriks, J.J.A. (2012). Myelin-derived lipids modulate macrophage activity by liver X receptor activation. PLoS One *7*, e44998.

Bogie, J.F.J., Grajchen, E., Wouters, E., Corrales, A.G., Dierckx, T., Vanherle, S., Mailleux, J., Gervois, P., Wolfs, E., Dehairs, J., et al. (2020). Stearoyl-CoA desaturase-1 impairs the reparative properties of macrophages and microglia in the brain. J. Exp. Med. *217*, e20191660.

Boven, L.A., Van Meurs, M., Van Zwam, M., Wierenga-Wolf, A., Hintzen, R.Q., Boot, R.G., Aerts, J.M., Amor, S., Nieuwenhuis, E.E., and Laman, J.D. (2006). Myelin-laden macrophages are anti-inflammatory, consistent with foam cells in multiple sclerosis. Brain *129*, 517–526.

Button, E.B., Boyce, G.K., Wilkinson, A., Stukas, S., Hayat, A., Fan, J., Wadsworth, B.J., Robert, J., Martens, K.M., and Wellington, C.L. (2019). ApoA-I deficiency increases cortical amyloid deposition, cerebral amyloid angiopathy, cortical and hippocampal astrogliosis, and amyloid-associated astrocyte reactivity in APP/PS1 mice. Alzheimer's Res. Ther. *11*, 44.

Camargo, N., Goudriaan, A., van Deijk, A.L.F., Otte, W.M., Brouwers, J.F., Lodder, H., Gutmann, D.H., Nave, K.A., Dijkhuizen, R.M., Mansvelder, H.D., et al. (2017). Oligodendroglial myelination requires astrocyte-derived lipids. PLoS Biol. *15*, e1002605.

Cantuti-Castelvetri, L., Fitzner, D., Bosch-Queralt, M., Weil, M.T., Su, M., Sen, P., Ruhwedel, T., Mitkovski, M., Trendelenburg, G., Lütjohann, D., et al. (2018). Defective cholesterol clearance limits remyelination in the aged central nervous system. Science *359*, 684–688.

Chinetti, G., Lestavel, S., Bocher, V., Remaley, A.T., Neve, B., Torra, I.P., Teissier, E., Minnich, A., Jaye, M., Duverger, N., et al. (2001). PPAR-alpha and PPAR-gamma activators induce cholesterol removal from human macrophage foam cells through stimulation of the ABCA1 pathway. Nat. Med. *7*, 53–58.

Chrast, R., Saher, G., Nave, K.A., and Verheijen, M.H.G. (2011). Lipid metabolism in myelinating glial cells: lessons from human inherited disorders and mouse models. J. Lipid Res. *52*, 419–434.

Coburn, C.T., Knapp, F.F., Jr., Febbraio, M., Beets, A.L., Silverstein, R.L., and Abumrad, N.A. (2000). Defective uptake and utilization of long chain fatty acids in muscle and adipose tissues of CD36 knockout mice. J. Biol. Chem. *275*, 32523–32529.

D'Ambrosio, D.N., Walewski, J.L., Clugston, R.D., Berk, P.D., Rippe, R.A., and Blaner, W.S. (2011). Distinct populations of hepatic stellate cells in the mouse liver have different capacities for retinoid and lipid storage. PLoS One *6*, e24993.

Dillenburg, A., Ireland, G., Holloway, R.K., Davies, C.L., Evans, F.L., Swire, M., Bechler, M.E., Soong, D., Yuen, T.J., Su, G.H., et al. (2018). Activin receptors regulate the oligodendrocyte lineage in health and disease. Acta Neuropathol. *135*, 887–906.

Drover, V.A., Nguyen, D.V., Bastie, C.C., Darlington, Y.F., Abumrad, N.A., Pessin, J.E., London, E., Sahoo, D., and Phillips, M.C. (2008). CD36 mediates both cellular uptake of very long chain fatty acids and their intestinal absorption in mice. J. Biol. Chem. *283*, 13108–13115.

Franklin, R.J.M., and Ffrench-Constant, C. (2017). Regenerating CNS myelin - from mechanisms to experimental medicines. Nat. Rev. Neurosci. *18*, 753–769.

Gou, S., Wang, L., Zhong, C., Chen, X., Ouyang, X., Li, B., Bao, G., Liu, H., Zhang, Y., and Ni, J. (2020). A novel apoA-I mimetic peptide suppresses atherosclerosis by promoting physiological HDL function in apoE(-/-) mice. Br. J. Pharmacol. *177*, 4627–4644.

Grajchen, E., Hendriks, J.J.A., and Bogie, J.F.J. (2018). The physiology of foamy phagocytes in multiple sclerosis. Acta Neuropathol. Commun. *6*, 124.

Grajchen, E., Wouters, E., van de Haterd, B., Haidar, M., Hardonnière, K., Dierckx, T., Van Broeckhoven, J., Erens, C., Hendrix, S., Kerdine-Römer, S., et al. (2020). CD36-mediated uptake of myelin debris by macrophages and microglia reduces neuroinflammation. J. Neuroinflammation *17*, 224.

Gu, Z., Li, F., Zhang, Y.P., Shields, L.B.E., Hu, X., Zheng, Y., Yu, P., Zhang, Y., Cai, J., Vitek, M.P., and Shields, C.B. (2013). Apolipoprotein E mimetic promotes functional and histological recovery in lysolecithin-induced spinal cord demyelination in mice. J. Neurol. Neurophysiol. *2014*, 10.

Haidar, M., Loix, M., Bogie, J.F.J., and Hendriks, J.J.A. (2021). Lipophagy: a new player in CNS disorders. Trends Endocrinol. Metab. *32*, 941–951.

Hames, K.C., Vella, A., Kemp, B.J., and Jensen, M.D. (2014). Free fatty acid uptake in humans with CD36 deficiency. Diabetes *63*, 3606–3614.

Hasbargen, K.B., Shen, W.J., Zhang, Y., Hou, X., Wang, W., Shuo, Q., Bernlohr, D.A., Azhar, S., and Kraemer, F.B. (2020). Slc43a3 is a regulator of free fatty acid flux. J. Lipid Res. *61*, 734–745.

Hesp, Z.C., Goldstein, E.Z., Goldstein, E.A., Miranda, C.J., Kaspar, B.K., Kaspar, B.K., and McTigue, D.M. (2015). Chronic oligodendrogenesis and remyelination after spinal cord injury in mice and rats. J. Neurosci. *35*, 1274–1290.

Hussain, R., El-Etr, M., Gaci, O., Rakotomamonjy, J., Macklin, W.B., Kumar, N., Sitruk-Ware, R., Schumacher, M., and Ghoumari, A.M. (2011). Progesterone and Nestorone facilitate axon remyelination: a role for progesterone receptors. Endocrinology *152*, 3820–3831.

Karamita, M., Barnum, C., Möbius, W., Tansey, M.G., Szymkowski, D.E., Lassmann, H., and Probert, L. (2017). Therapeutic inhibition of soluble brain TNF promotes remyelination by increasing myelin phagocytosis by microglia. JCI Insight *2*, 87455.

Karten, B., Campenot, R.B., Vance, D.E., and Vance, J.E. (2006). Expression of ABCG1, but not ABCA1, correlates with cholesterol release by cerebellar astroglia. J. Biol. Chem. *281*, 4049–4057.

Keough, M.B., Rogers, J.A., Zhang, P., Jensen, S.K., Stephenson, E.L., Chen, T., Hurlbert, M.G., Lau, L.W., Rawji, K.S., Plemel, J.R., et al. (2016). An inhibitor of chondroitin sulfate proteoglycan synthesis promotes central nervous system remyelination. Nat. Commun. *7*, 11312.

Lada, A.T., Willingham, M.C., and St Clair, R.W. (2002). Triglyceride depletion in THP-1 cells alters cholesteryl ester physical state and cholesterol efflux. J. Lipid Res. *43*, 618–628.

Lampron, A., Larochelle, A., Laflamme, N., Préfontaine, P., Plante, M.M., Sánchez, M.G., Yong, V.W., Stys, P.K., Tremblay, M.È., and Rivest, S. (2015). Inefficient clearance of myelin debris by microglia impairs remyelinating processes. J. Exp. Med. *212*, 481–495.

Lan, M., Tang, X., Zhang, J., and Yao, Z. (2018). Insights in pathogenesis of multiple sclerosis: nitric oxide may induce mitochondrial dysfunction of oligodendrocytes. Rev. Neurosci. *29*, 39–53.

Lewis, T.L., Cao, D., Lu, H., Mans, R.A., Su, Y.R., Jungbauer, L., Linton, M.F., Fazio, S., LaDu, M.J., and Li, L. (2010). Overexpression of human apolipoprotein A-I preserves cognitive function and attenuates neuroinflammation and cerebral amyloid angiopathy in a mouse model of Alzheimer disease. J. Biol. Chem. *285*, 36958–36968.

Liu, D., Ding, Z., Wu, M., Xu, W., Qian, M., Du, Q., Zhang, L., Cui, Y., Zheng, J., Chang, H., et al. (2017). The apolipoprotein A-I mimetic peptide, D-4F, alleviates ox-LDL-induced oxidative stress and promotes endothelial repair through the eNOS/HO-1 pathway. J. Mol. Cell. Cardiol. *105*, 77–88.

Liu, L., Zhang, K., Sandoval, H., Yamamoto, S., Jaiswal, M., Sanz, E., Li, Z., Hui, J., Graham, B.H., Quintana, A., and Bellen, H.J. (2015). Glial lipid droplets and ROS induced by mitochondrial defects promote neurodegeneration. Cell *160*, 177–190.

Makinodan, M., Ikawa, D., Miyamoto, Y., Yamauchi, J., Yamamuro, K., Yamashita, Y., Toritsuka, M., Kimoto, S., Okumura, K., Yamauchi, T., et al. (2016). Social isolation impairs remyelination in mice through modulation of IL-6. Faseb j *30*, 4267–4274.

Marschallinger, J., Iram, T., Zardeneta, M., Lee, S.E., Lehallier, B., Haney, M.S., Pluvinage, J.V., Mathur, V., Hahn, O., Morgens, D.W., et al. (2020). Lipid-droplet-accumulating microglia represent a dysfunctional and proinflammatory state in the aging brain. Nat. Neurosci. *23*, 194–208.

McMahon, E.J., Suzuki, K., and Matsushima, G.K. (2002). Peripheral macrophage recruitment in cuprizone-induced CNS demyelination despite an intact blood-brain barrier. J. Neuroimmunol. *130*, 32–45.

Meffre, D., Massaad, C., and Grenier, J. (2015). Lithium chloride stimulates PLP and MBP expression in oligodendrocytes via Wnt/β-catenin and Akt/CREB pathways. Neuroscience *284*, 962–971.

Meriwether, D., Sulaiman, D., Wagner, A., Grijalva, V., Kaji, I., Williams, K.J., Yu, L., Fogelman, S., Volpe, C., Bensinger, S.J., et al. (2016). Transintestinal transport of the antiinflammatory drug 4F and the modulation of transintestinal cholesterol efflux. J. Lipid Res. *57*, 1175–1193.

Miron, V.E., Boyd, A., Zhao, J.W., Yuen, T.J., Ruckh, J.M., Shadrach, J.L., van Wijngaarden, P., Wagers, A.J., Williams, A., Franklin, R.J.M., and Ffrench-Constant, C. (2013). M2 microglia and macrophages drive oligodendrocyte differentiation during CNS remyelination. Nat. Neurosci. *16*, 1211–1218.

Nanjee, M.N., Crouse, J.R., King, J.M., Hovorka, R., Rees, S.E., Carson, E.R., Morgenthaler, J.J., Lerch, P., and Miller, N.E. (1996). Effects of intravenous infusion of lipid-free apo A-I in humans. Arterioscler. Thromb. Vasc. Biol. *16*, 1203–1214.

Navab, M., Anantharamaiah, G.M., Reddy, S.T., Hama, S., Hough, G., Grijalva, V.R., Wagner, A.C., Frank, J.S., Datta, G., Garber, D., and Fogelman, A.M. (2004). Oral D-4F causes formation of pre-beta high-density lipoprotein and improves high-density lipoprotein-mediated cholesterol efflux and reverse cholesterol transport from macrophages in apolipoprotein E-null mice. Circulation *109*, 3215–3220.

Nissen, S.E. (2005). Effect of intensive lipid lowering on progression of coronary atherosclerosis: evidence for an early benefit from the Reversal of Atherosclerosis with Aggressive Lipid Lowering (REVERSAL) trial. Am. J. Cardiol. *96*, 61f–68f.

Nowacki, T.M., Remaley, A.T., Bettenworth, D., Eisenblätter, M., Vowinkel, T., Becker, F., Vogl, T., Roth, J., Tietge, U.J., Lügering, A., et al. (2016). The 5A apolipoprotein A-I (apoA-I) mimetic peptide ameliorates experimental colitis by regulating monocyte infiltration. Br. J. Pharmacol. *173*, 2780–2792.

Peng, H., Bria, A., Zhou, Z., Iannello, G., and Long, F. (2014). Extensible visualization and analysis for multidimensional images using Vaa3D. Nat. Protoc. *9*, 193–208.

Peterson, S.J., Husney, D., Kruger, A.L., Olszanecki, R., Ricci, F., Rodella, L.F., Stacchiotti, A., Rezzani, R., McClung, J.A., Aronow, W.S., et al. (2007). Long-term treatment with the apolipoprotein A1 mimetic peptide increases antioxidants and vascular repair in type I diabetic rats. J. Pharmacol. Exp. Ther. *322*, 514–520.

Pohl, J., Ring, A., Korkmaz, U., Ehehalt, R., and Stremmel, W. (2005). FAT/CD36-mediated long-chain fatty acid uptake in adipocytes requires plasma membrane rafts. Mol. Biol. Cell *16*, 24–31.

Rosenbaum, M.A., Chaudhuri, P., Abelson, B., Cross, B.N., and Graham, L.M. (2015). Apolipoprotein A-I mimetic peptide reverses impaired arterial healing after injury by reducing oxidative stress. Atherosclerosis *241*, 709–715.

Schwendeman, A., Sviridov, D.O., Yuan, W., Guo, Y., Morin, E.E., Yuan, Y., Stonik, J., Freeman, L., Ossoli, A., Thacker, S., et al. (2015). The effect of phospholipid composition of reconstituted HDL on its cholesterol efflux and antiinflammatory properties. J. Lipid Res. *56*, 1727–1737.

Sengupta, M.B., Saha, S., Mohanty, P.K., Mukhopadhyay, K.K., and Mukhopadhyay, D. (2017). Increased expression of ApoA1 after neuronal injury may be beneficial for healing. Mol. Cell. Biochem. *424*, 45–55.

Sethi, A.A., Stonik, J.A., Thomas, F., Demosky, S.J., Amar, M., Neufeld, E., Brewer, H.B., Davidson, W.S., D'Souza, W., Sviridov, D., and Remaley, A.T. (2008). Asymmetry in the lipid affinity of bihelical amphipathic peptides. A structural determinant for the specificity of ABCA1-dependent cholesterol efflux by peptides. J. Biol. Chem. *283*, 32273–32282.

Shelestak, J., Singhal, N., Frankle, L., Tomor, R., Sternbach, S., McDonough, J., Freeman, E., and Clements, R. (2020). Increased blood-brain barrier hyperpermeability coincides with mast cell activation early under cuprizone administration. PLoS One *15*, e0234001.

Sherman, C.B., Peterson, S.J., and Frishman, W.H. (2010). Apolipoprotein A-I mimetic peptides: a potential new therapy for the prevention of atherosclerosis. Cardiol. Rev. *18*, 141–147.

Stamatikos, A., Dronadula, N., Ng, P., Palmer, D., Knight, E., Wacker, B.K., Tang, C., Kim, F., and Dichek, D.A. (2019). ABCA1 overexpression in endothelial cells in vitro enhances ApoAI-mediated cholesterol efflux and decreases inflammation. Hum. Gene Ther. *30*, 236–248.

Stangel, M., Kuhlmann, T., Matthews, P.M., and Kilpatrick, T.J. (2017). Achievements and obstacles of remyelinating therapies in multiple sclerosis. Nat. Rev. Neurol. *13*, 742–754.

Sviridov, D.O., Andrianov, A.M., Anishchenko, I.V., Stonik, J.A., Amar, M.J.A., Turner, S., and Remaley, A.T. (2013). Hydrophobic amino acids in the hinge region of the 5A apolipoprotein mimetic peptide are essential for promoting cholesterol efflux by the ABCA1 transporter. J. Pharmacol. Exp. Ther. *344*, 50–58.

Swaminathan, S.K., Zhou, A.L., Ahlschwede, K.M., Curran, G.L., Lowe, V.J., Li, L., and Kandimalla, K.K. (2020). High-density lipoprotein mimetic peptide 4F efficiently crosses the blood-brain barrier and modulates amyloid-β distribution between brain and plasma. J. Pharmacol. Exp. Ther. *375*, 308–316.

Tabet, F., Remaley, A.T., Segaliny, A.I., Millet, J., Yan, L., Nakhla, S., Barter, P.J., Rye, K.A., and Lambert, G. (2010). The 5A apolipoprotein A-I mimetic peptide displays antiinflammatory and antioxidant properties in vivo and in vitro. Arterioscler. Thromb. Vasc. Biol. *30*, 246–252.

Tang, C., Liu, Y., Kessler, P.S., Vaughan, A.M., and Oram, J.F. (2009). The macrophage cholesterol exporter ABCA1 functions as an antiinflammatory receptor. J. Biol. Chem. *284*, 32336–32343.

Tang, C., Vaughan, A.M., and Oram, J.F. (2004). Janus kinase 2 modulates the apolipoprotein interactions with ABCA1 required for removing cellular cholesterol. J. Biol. Chem. *279*, 7622–7628.

Thiam, A.R., and Beller, M. (2017). The why, when and how of lipid droplet diversity. J. Cell Sci. *130*, 315–324.

Thiam, A.R., Farese, R.V., Jr., and Walther, T.C. (2013). The biophysics and cell biology of lipid droplets. Nat. Rev. Mol. Cell Biol. *14*, 775–786.

Vaughan, A.M., and Oram, J.F. (2003). ABCA1 redistributes membrane cholesterol independent of apolipoprotein interactions. J. Lipid Res. *44*, 1373–1380.

Vazquez, M.M., Gutierrez, M.V., Salvatore, S.R., Puiatti, M., Dato, V.A., Chiabrando, G.A., Freeman, B.A., Schopfer, F.J., and Bonacci, G. (2020). Nitro-oleic acid, a ligand of CD36, reduces cholesterol accumulation by modulating oxidized-LDL uptake and cholesterol efflux in RAW264.7 macrophages. Redox Biol. *36*, 101591.

Vela, J.M., Molina-Holgado, E., Arévalo-Martín, A., Almazán, G., and Guaza, C. (2002). Interleukin-1 regulates proliferation and differentiation of oligodendrocyte progenitor cells. Mol. Cell. Neurosci. *20*, 489–502.

Vereecke, L., Vieira-Silva, S., Billiet, T., van Es, J.H., Mc Guire, C., Slowicka, K., Sze, M., van den Born, M., De Hertogh, G., Clevers, H., et al. (2014). A20 controls intestinal homeostasis through cell-specific activities. Nat. Commun. *5*, 5103.

Yao, X., Dai, C., Fredriksson, K., Dagur, P.K., McCoy, J.P., Qu, X., Yu, Z.X., Keeran, K.J., Zywicke, G.J., Amar, M.J.A., et al. (2011). 5A, an apolipoprotein A-I mimetic peptide, attenuates the induction of house dust mite-induced asthma. J. Immunol. *186*, 576–583.

Zhao, G.J., Yin, K., Fu, Y.C., and Tang, C.K. (2012). The interaction of ApoA-I and ABCA1 triggers signal transduction pathways to mediate efflux of cellular lipids. Mol. Med. *18*, 149–158.

STAR★METHODS

KEY RESOURCES TABLE

REAGENT or RESOURCE	SOURCE	IDENTIFIER
Antibodies		
Rabbit anti-NF	Abcam	Cat. #ab8135; RRID: AB_306298
Rat anti-MBP	Millipore	Cat. #MAB386; RRID: AB_94975
Rabbit anti-dMBP	Sigma-Aldrich	Cat. #ab5864; RRID: AB_2140351
Rat anti-F4/80	Bio-Rad	Cat. #MCA497G; RRID: AB_872005
Rabbit anti-PLIN2	Abcam	Cat. #ab52356; RRID: AB_2223599
Rabbit anti-LC3	Sigma-Aldrich	Cat. #L7543; RRID: AB_796155
Rabbit anti-p62	Cell Signaling Technology	Cat. #23214; RRID: AB_2798858
Rabbit anti-CD36	Abcam	Cat. #ab124515; RRID: AB_2924667
Goat anti-rabbit IgG Alexa Fluor 488	Invitrogen	Cat. #A11008; RRID: AB_143165
Goat anti-rat IgG Alexa Fluor 555	Invitrogen	Cat. #A21434; RRID: AB_141733
Goat anti-rabbit IgG Alexa Fluor 555	Invitrogen	Cat. #A21430; RRID: AB_10374475
Goat anti-rat IgG Alexa Fluor 647	Invitrogen	Cat. #A21247; RRID: AB_141778
Chemicals, peptides, and recombinant proteins		
Bis(cyclohexanone)oxaldihydrazone	Sigma-Aldrich	Cat. #C9012
Peptide 5A	Dr. Alan Remaley	N/A
BODIPY (493/503)	Invitrogen	Cat. #D3922
Vybrant DiI Cell)labeling solution	Thermofisher	Cat. #V22885
Latex beads	Sigma-Aldrich	Cat. #L3030
IFNg	Peprotech	Cat. #315-05
IL1b	Peprotech	Cat. #211-11b
Simvastatin	Sigma-Aldrich	Cat. #S6196
TOFA	Sigma-Aldrich	Cat. #T6575
C75	MedChemExpress	Cat. #HY-12364
AG490	MedChemExpress	Cat. #HY-12000
Critical commercial assays		
RNeasy mini kit	Qiagen	Cat. #74106
qScript cDNA synthesis kit	Quantabio	Cat. #7331178
SYBR Green	Thermo Fisher	Cat. #106631376
Amplex Red Cholesterol Assay kit	Thermo Fisher	Cat. #A12216
Experimental models: Organisms/strains		
Wild-type C57BL/6J *Mus Musculus*	Envigo	N/A
Abca1 $^{-/-}$ C57BL/6J *Mus Musculus*	In house	N/A
LysmCre C57BL/6J *Mus Musculus*	Prof. dr. Geert van Loo (University of Ghent)	N/A
Cd36 $^{-/-}$ C57BL/6J *Mus Musculus*	The Jackson Laboratories	Cat. #JAX:019,006
Oligonucleotides		
For primers, see Table S1	N/A	N/A
Software and algorithms		
ImageJ	https://imagej.net/Welcome	N/A
Graphpad Prism	https://www.graphpad.com:443/	N/A

RESOURCE AVAILABILITY

Lead contact

Further information and requests for resources and reagents should be directed to and will be fulfilled by the Lead Contact, Jeroen Bogie (jeroen.bogie@uhasselt.be).

Materials availability

This study did not generate new unique reagents.

Data and code availability

- All data reported in this paper will be shared by the lead contact upon request.
- This paper does not report original code.
- Any additional information required to reanalyze the data reported in this paper is available from the lead contact upon request.

EXPERIMENTAL MODEL AND SUBJECT DETAILS

Animals

Wild-type C57BL/6J mice were purchased from Envigo. *Cd36*$^{-/-}$ mice were purchased from the Jackson Laboratory. To generate C57BL/6J phagocyte-specific *Abca1*$^{-/-}$ mice, C57BL/6J *Abca1*$^{fl/fl}$ mice were crossbred with C57BL/6J *LysM*^{Cre} mice, which were kindly provided by prof. dr. Geert van Loo (VIB-UGent Center for inflammation Research, University of Ghent, Belgium) (Vereecke et al., 2014). Mice were housed on a 12h light/dark cycle with *ad libitum* access to water and a standard chow diet or specific formulations as indicated. All animal procedures were conducted in accordance with the institutional guidelines and approved by the Ethical Committee for Animal Experiments of Hasselt University (protocol numbers 201963K, 201964, and 201304A2).

Cuprizone-induced acute demyelination *in vivo* model

To induce acute demyelination, 9-11-week-old male mice were fed *ad libitum* a diet containing 0.3% (w/w) cuprizone (bis[cyclohexanone]oxaldihydrazone, Sigma-Aldrich) mixed in powdered standard chow for 6 weeks. After the withdrawal of the cuprizone diet, mice were fed powdered standard chow for 1 week. After 4 weeks of cuprizone diet, mice were daily injected intraperitoneally with either 30 mg/kg peptide 5A or vehicle until sacrifice. After 6 weeks or 7 weeks from start of cuprizone diet, mice were sacrificed, and tissue was collected for histological and biochemical analysis.

Experimental autoimmune encephalomyelitis

At the age of 12 weeks, female wild-type C57BL/6J mice were immunized subcutaneously with 200 μg of recombinant human myelin oligodendrocyte glycoprotein peptide 35–55, emulsified in complete Freund's adjuvant supplemented with 4 mg/mL of *Mycobacterium tuberculosis* according to manufacturer's guidelines (Hooke Laboratories). Directly after immunization and after 24h, mice were injected intraperitoneally with 100 ng pertussis toxin. Mice were weighed and clinically scored for neurological signs of the disease on a daily basis following a five-point standardized rating of clinical symptoms: 0: no clinical symptoms; 1: tail paralysis; 2: tail paralysis and partial hindlimb paralysis; 3: complete hindlimb paralysis; 4: paralysis to the diaphragm; 5: death by EAE. Starting from day 5 post-immunization, animals were injected intraperitoneally with peptide 5A (30 mg/kg) or vehicle on a daily basis.

Cerebellar brain slice cultures

Cerebellar brain slices were obtained from wild-type C57BL/6J mouse pups at postnatal day 10, as described previously (Hussain et al., 2011; Meffre et al., 2015). Brain slices were cultured in MEM medium (Thermo Fisher Scientific) supplemented with 25% horse serum (Thermo Fisher Scientific), 25% Hank's balanced salt solution (Sigma-Aldrich), 50 U/mL penicillin (Invitrogen), 50 U/mL streptomycin (Invitrogen), 1% Glutamax (Thermo Fisher Scientific), 12.5 mM HEPES (Thermo Fisher Scientific), and 1.45 g/L glucose (Sigma-Aldrich). To deplete microglia, slices were treated for 24 h with empty or clodronate liposomes (0.5 mg/mL, LIPOSOMA) immediately after isolation. To induce demyelination, brain slices were treated with 0.5 mg/mL lysolecithin (Sigma-Aldrich) at 3 days post isolation for 16h. Next, brain slices were allowed to recover in culture medium for 1 day and subsequently treated daily with 50 μg/mL peptide 5A or vehicle for 1 week, followed by histological and biochemical analysis.

Cell isolation and culture

BMDMs were obtained as described previously (Bogie et al., 2017). Briefly, femoral and tibial bone marrow was isolated from 11-week-old female wild-type, *Abca1*$^{-/-}$ and *Cd36*$^{-/-}$ C57BL/6J mice and cultured in 14.5 cm petri dishes (Greiner, ref. 639,161) at a concentration of 10 x 10^6 cells/Petri dish in RPMI1640 medium (Lonza) supplemented with 10% fetal calf serum (FCS; Biowest), 50 U/mL penicillin (Invitrogen), 50 U/mL streptomycin (Invitrogen), and 15% L929-conditioned medium (LCM) for 7 days. Next, cells were cultured at a density of 0.5 x 10^6 cells/mL in RPMI 1640 supplemented with 10% FCS, 50 U/mL penicillin, 50 U/mL streptomycin, and 5% LCM. Microglia were obtained from the cortices of postnatal day 1–3 wild-type and *Cd36*$^{-/-}$ C57BL/6J mice and cultured in a T75 flask (Greiner) in high-glucose DMEM medium (Gibco), supplemented with 10% FCS, 50 U/mL penicillin and 50 U/mL streptomycin. 3 days after isolation, cultures were supplemented with 33% LCM. After 14 days, microglia were collected by means of the orbital shake-off method (230 rpm, 3h), after which the cells were cultured at a density of 0.5 x 10^6 cells/mL in high-glucose DMEM supplemented with 10% FCS, 50 U/mL penicillin, 50 U/mL streptomycin, and 15% LCM. BMDMs and microglia were treated daily with 10 μg/mL peptide 5A, 100 μg/mL myelin, and/or 25 μM AG490 for 24h or 72h. For phenotyping, BMDMs and microglia were stimulated with IFN-γ and IL-1β (both 100 ng/mL) for 6h to assess gene expression.

Myelin isolation

Myelin was purified from postmortem mouse brain tissue of 11-week-old male and female C57BL6/J mice by means of density gradient centrifugation, as described previously (Bogie et al., 2017). Briefly, brain tissue was homogenized in 0.32M sucrose and subsequently layered on top of 0.85M sucrose. After centrifugation at 75,000g, myelin was collected from the interface and washed and purified in water. Myelin protein concentration was determined using the BCA protein assay kit (Thermo Fisher Scientific), according to the manufacturer's guidelines.

METHOD DETAILS

Antibodies and chemical reagents

The following antibodies were used for immunofluorescent/immunohistochemical stainings: anti-NF (1:1000, cat. #ab8135, Abcam), anti-MBP (1:250, cat. #MAB386, Millipore), anti-dMBP (1:2000, cat. #ab5864, Sigma-Aldrich), anti-F4/80 (1:100, cat. #MCA497G, Bio-Rad), anti-PLIN2 (1:500, ab52356, Abcam), anti-LC3 (1:500, cat. #L7543, Sigma-Aldrich), anti-p62 (1:500, cat. #23214, Cell Signaling Technology), anti-CD36 (1:100, cat. #ab124515, Abcam). Appropriate secondary antibodies were purchased from Invitrogen. BODIPY (493/503) was used to fluorescently label lipid droplets (2 μM, cat. #D3922, Invitrogen). Simvastatin (2 μM, cat. #S6196, Sigma-Aldrich), TOFA (10 μg/mL, cat. #T6575, Sigma-Aldrich), C75 (25 μM, cat. #HY-12364, MedChemExpress), and AG490 (25 μM, cat. #HY-12000, MedChemExpress) were used to inhibit HMG-CoA reductase, ACC1, FASN, and JAK2/STAT3, respectively. Interferon-gamma (IFN-γ, 100 ng/mL, Peprotech) and interleukin-1 beta (IL-1β, 100 ng/mL, Peprotoch) were used to stimulate cells for inflammatory phenotyping.

Peptide 5A

Peptide 5A was kindly provided by dr. Remaley in a PBS solution (National Institute of Health). Briefly, peptide 5A contains 2 helices with amino acid sequences DWLKAFYDKVAEKLKEAF and DWAKAAYDKAAEKAKEAA, which are connected by a proline. The peptide is manufactured using a solid-phase procedure using a fluorenylmethyloxycarbonyl protocol on the Biosearch 9600 peptide synthesizer. By reverse phase high-performance liquid chromatography on an Aquapore RP-300 column, the peptide was purified to at least 99% purity. Finally, peptide 5A was reconstistuted with sphingomyelin (5A-SM; 1:3.5M ratio) to increase the efficacy of peptide 5A uptake (Amar et al., 2010; Sethi et al., 2008).

Myelin phagocytosis

BMDMs and microglia were treated with 100 μg/mL myelin. In order to evaluate the ability and extent of myelin phagocytosis, myelin was fluorescently labeled with 1,1′-dioctadecyl-3,3,3′,3′-tetramethylindocarbocyanine perchlorate (DiI, Sigma-Aldrich). BMDMs and microglia were exposed to 100 μg/mL DiI-labelled myelin for 1.5h and analyzed for fluorescence intensity by using the FACS Calibur (BD Biosciences). In order to define the uptake of latex beads, cells were exposed to fluorescent red latex beads for 1.5h (1:100, cat. No. L3030, Sigma-Aldrich). Data is represented as relative phagocytosis compared to vehicle.

Quantitative PCR

Tissue or cells were lysed using QIAzol reagent (Qiagen). Next, RNA was extracted using the RNeasy mini kit (Qiagen) according to the manufacturer's instructions. cDNA was synthesized using the qScript cDNA synthesis kit (Quanta Biosciences) according to the manufacturer's instructions. Quantitative PCR was performed on a StepOnePlus detection system (Applied Biosystems). Data were analyzed using the comparative Ct method and normalized to the most stable reference genes as determined by GeNorm, being *Cyca* and *Rpl13a* for RNA isolated out of cerebellar brain slices and corpus callosum tissue of cuprizone animals, and *Cyca* and *Tbp* for RNA isolated out of BMDMs and microglia. Primer sequences are summarized in Table S1.

Immunofluorescence

Murine BMDMs were cultured on glass cover slides and fixed in 4% paraformaldehyde (PFA) for 20 min on room temperature or ice-cold methanol for 10 min (LC3/p62 staining). Cerebellar brain slices were fixed in 4% PFA for 15 min on room temperature. Brain tissue of cuprizone mice was isolated, snap-frozen, and sectioned with a Leica CM1900UV cryostat (Leica Microsystems) to obtain 10 μm slices. Cryosections were fixed in ice-cold acetone for 10 min at −20°C. Immunostaining and analysis of cryosections were performed as described previously (Bogie et al., 2017). Briefly, cryosections were incubated with the primary antibodies overnight at 4°C. After washing, cyrosetions were incubated with the relevant secondary antibodies for 1h at room temperature. ImageJ was used to align the corpus callosum followed by determination of the MBP or dMBP positive signal in this area. To stain cerebellar brain slices, samples were incubated with relevant primary antibodies diluted in blocking buffer (1x PBS +5% horse serum +0.3% Triton X-100), eventually followed by a 30 min incubation with BODIPY. Analysis of cerebellar brain slices and BMDM cultures were performed using the LSM 880 confocal microscope (Zeiss). ImageJ was used to determine the dMBP positive area in the cerebellar brain slices, which is presented as the relative $dMBP^+$ area compared to vehicle, and to define the myelination index (MBP^+ NF^+ axons/NF^+ axons) which is presented in a relative normalized manner. Three-dimensional analysis of cerebellar brain slices was performed using the z stack feature, and images were 3D rendered using the 3D rendering

software vaa3d (Peng et al., 2014). For BMDM images, the AIRYscan feature was used. Images shown in figures are digitally enhanced. All analyses were conducted by observers blinded to the experimental arm of the study.

Oil Red O staining

To visualize intracellular myelin degradation products, unfixed cryosections, cerebellar brain slices, and fixed BMDMs were stained with 0.3% Oil Red O (Sigma-Aldrich) for 10 min. Cryosections and BMDMs were counterstained with hematoxylin (Merck). Images were acquired using a Leica DM 2000 LED microscope. Alternatively, a quantitative analysis was performed by measuring absorbance at 540 nm using a microplate reader (iMark, Bio-Rad). For cryosections, ImageJ was used to align the corpus callosum and to determine the ORO positive area in this alignment. For cerebellar brain slices, ImageJ was used to determine the ORO positive area in the cerebellar brain slices, which is presented as the relative ORO^+ area compared to vehicle. All analyses were conducted by observers blinded to the experimental arm of the study.

Flow cytometry

BMDMs and microglia were stained for intracellular lipid load by 15 min incubation with BODIPY (493/503) at 37°C. The FACSCalibur was used to quantify cellular fluorescence. Data is represented as relative lipid droplet load compared to vehicle.

Transmission electron microscopy

Mice brain samples were fixed with 2% glutaraldehyde. Next, post-fixation was done with 2% osmiumtetroxide in 0.05M sodium cacodylate buffer for 1h at 4°C. Dehydration of the samples was performed by ascending concentrations of acetone. Afterward, the dehydrated samples were impregnated overnight in a 1:1 mixture of acetone and araldite epoxy resin. Next, the samples were embedded in araldite epoxy resin at 60°C and were cut in slices of 70 nm, perpendicular to the corpus callosum, with a Leica EM UC6 microtome. The slices were transferred to 0.7% formvar-coated copper grids (Aurion). Afterward, the samples were contrasted with 0.5% uranyl acetate and lead citrate using a Leica EM AC20. Analysis was performed with a Philips EM208 S electron microscope (Philips) equipped with a Morada Soft Imaging System camera with iTEM-FEI software (Olympus SIS). ImageJ was used to calculate the g-ratio (ratio of the inner axonal diameter to the total outer diameter). All analyses were conducted by observers blinded to the experimental arm of the study.

Cholesterol measurements

Cholesterol levels of BMDMs and microglia were defined by using the Amplex Red Cholesterol Assay kit (Thermo Fisher) according to the manufacturer's instructions. To determine the cholesterol efflux of BMDMs and microglia, BMDM and microglia cultures were first treated with myelin for 72h and then exposed to peptide 5A (50 μg/mL) in phenol- and serum-free medium for 4h before measuring the intra- and extracellular total cholesterol levels using the Amplex Red Cholesterol Assay kit. Fluorescence was measured using the FLUOstar OPTIMA microplate reader, and cholesterol efflux was determined by dividing fluorescence in the supernatants by the total fluorescence in supernatants and cells.

LC-ESI-MS/MS

BMDM cell pellets were diluted in 700 μL 1x PBS with 800 μL 1 N HCl:CH_3OH 1:8 (v/v), 900 μL $ChCl_3$ and 200 μg/mL of the antioxidant 2,6-di-tert-butyl-4-methylphenol (BHT; Sigma-Aldrich). 3 μL of SPLASH LIPIDOMIX Mass Spec Standard (Avanti Polar Lipids) was added to the extract mix. The organic fraction was evaporated at room temperature using the Savant Speedvac spd111v (Thermo Fisher), and the remaining lipid pellet was reconstituted in 100% ethanol. Lipid species were analyzed by liquid chromatography electrospray ionization tandem mass spectrometry (LC-ESI-MS/MS) on a Nexera X2 UHPLC system (Shimadzu) coupled with hybrid triple quadrupole/linear ion trap mass spectrometer (6500 + QTRAP system; AB SCIEX). Chromatographic separation was performed on a XBridge amide column (150 mm × 4.6 mm, 3 × 5 μm; Waters) maintained at 35°C using mobile phase A [1 mM ammonium acetate in water-acetonitrile 5:95 (v/v)] and mobile phase B [1 mM ammonium acetate in water-acetonitrile 50:50 (v/v)] in the following gradient: (0–6 min: 0% B → 6% B; 6–10 min: 6% B → 25% B; 10–11 min: 25% B → 98% B; 11–13 min: 98% B → 100% B; 13–19 min: 100% B; 19–24 min: 0% B) at a flow rate of 0.7 mL/min which was increased to 1.5 mL/min from 13 min onwards. Sphingomyelin (SM) and cholesteryl esters (CE) were measured in positive ion mode with a precursor scan of 184.1 and 369.4. Triglycerides (TG), diglycerides, and monoglycerides were measured in positive ion mode with a neutral loss scan for one of the fatty acyl moieties. Phosphatidylcholine (PC), phosphatidylethanolamine (PE), phosphatidylinositides (PI), and phosphatidylserines (PS) were measured in negative ion mode by fatty acyl fragment ions. Lipid quantification was performed by scheduled multiple reactions monitoring, the transitions being based on the neutral losses or the typical product ions as described above. The instrument parameters were as follows: Curtain Gas = 35 psi; Collision Gas = 8 a.u. (medium); IonSpray Voltage = 5500 V and −4500 V; Temperature = 550°C; Ion Source Gas 1 = 50 psi; Ion Source Gas 2 = 60 psi; Declustering Potential = 60 V and −80 V; Entrance Potential = 10 V and −10 V; Collision Cell Exit Potential = 15 V and −15 V. Peak integration was performed with the Multiquant TM software version 3.0.3. Lipid species signals were corrected for isotopic contributions (calculated with Python Molmass, 2019.1.1) and were quantified based on internal standard signals and adhere to the guidelines of the Lipidomics Standards Initiative. Only the detectable lipid classes and fatty acyl moieties are reported in this manuscript.

QUANTIFICATION AND STATISTICAL ANALYSIS

Statistical analysis

Data were statistically analyzed using GraphPad Prism v8 and are reported as mean ± s.e.m.. The number of animals and experimental replicates is indicated in the Figure legends. Data collection was randomized for all experiments. The D'Agostino and Pearson omnibus normality test was used to test for normal distribution. When datasets were normally distributed, an ANOVA (Tukey's post hoc analysis) or two-tailed unpaired Student's *t*-test (with Welch's correction if necessary) was used to determine statistical significance between groups. If datasets did not pass normality, the Kruskal-Wallis or Mann-Whitney analysis was applied. p values < 0.05 were considered to indicate a significant difference (*, $p < 0.05$; **, $p < 0.01$; ***, $p < 0.001$; ****, $p < 0.0001$).

Cell Reports, Volume *41*

Supplemental information

The ApoA-I mimetic peptide 5A enhances remyelination by promoting clearance and degradation of myelin debris

Sam Vanherle, Winde Jorissen, Tess Dierckx, Melanie Loix, Elien Grajchen, Fleur Mingneau, Jeroen Guns, Pascal Gervois, Ivo Lambrichts, Jonas Dehairs, Johannes V. Swinnen, Monique T. Mulder, Alan T. Remaley, Mansour Haidar, Jerome J.A. Hendriks, and Jeroen J.F. Bogie

Supplementary figures and tables

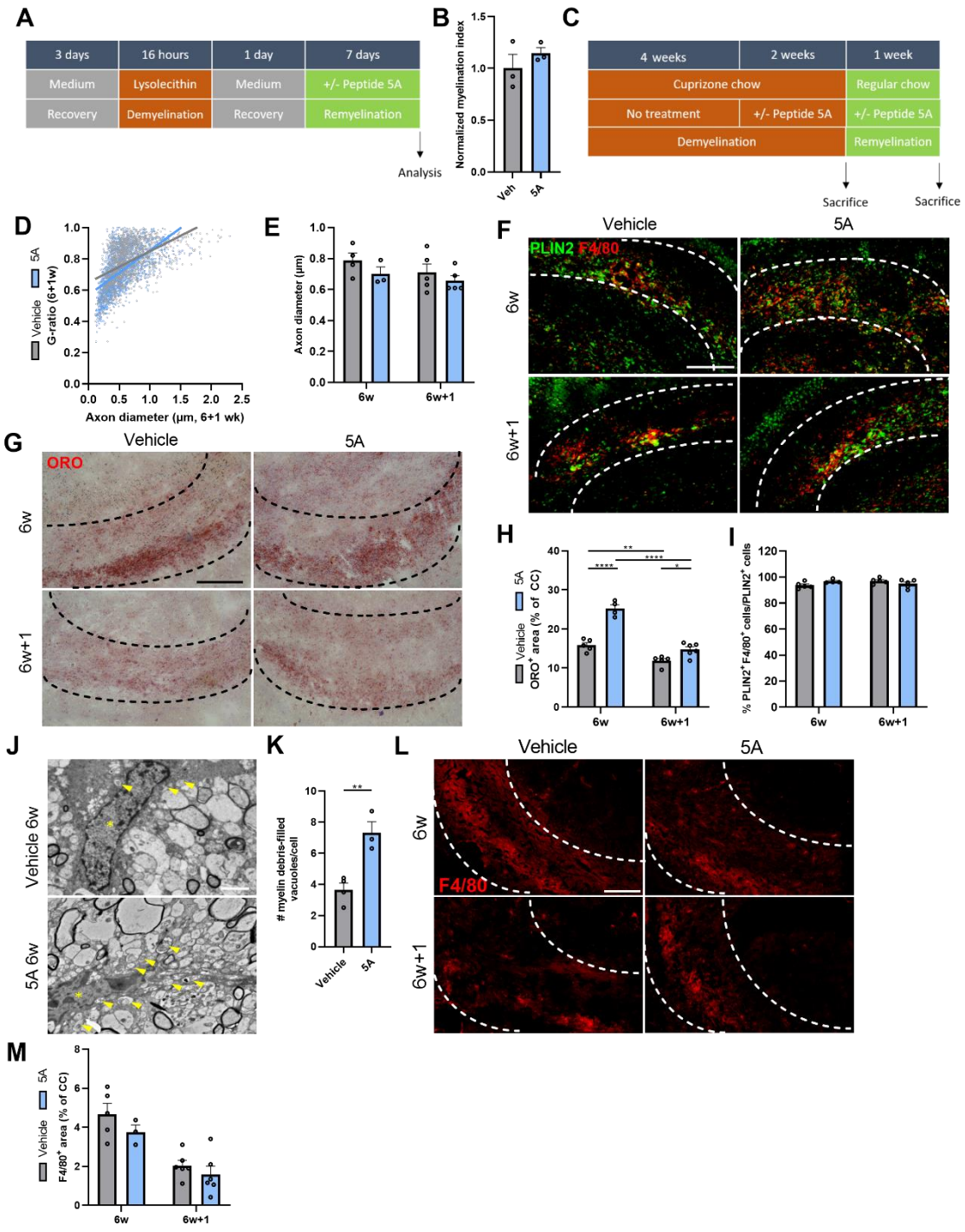

Figure S1: Peptide 5A does not influence phagocyte numbers in the corpus callosum of cuprizone fed mice, related to figures 1 & 2. A) Experimental setup of the cerebellar brain slice model. B) Normalized quantification of MBP$^+$ NF$^+$ axons out of total NF$^+$ axons in cerebellar brain slices treated with vehicle or peptide 5A during lysolecithin-induced demyelination (n = 3 slices). C) Experimental setup of the cuprizone model. D-E) Analysis of the g-ratio as a function of axon diameter (D) and of the axon diameter (E) in CC from vehicle- and peptide 5A (30 mg/kg)-treated mice after cuprizone-induced demyelination (6w) and remyelination (6w+1) (n = 3-5 animals). F) Representative images of immunofluorescence PLIN2/F4/80 staining of

the CC from vehicle- and peptide 5A-treated mice after 6w and 6w+1. Scale bar, 200µm. G-H) Representative images of Oil red O (ORO) staining (G) and quantification of the ORO^+ area (H) of the CC from vehicle- and peptide 5A-treated mice after 6w and 6w+1. Scale bar, 200 µm (n = 4-6 animals). I) Quantification of the ratio of $PLIN2^+$ $F4/80^+$ cells/$PLIN2^+$ cells in CC from vehicle- and peptide 5A-treated mice after 6w and 6w+1 (n = 4-5 animals). J) Transmission electron microscopy analysis of the corpus callosum (CC) from vehicle- and peptide 5A-treated mice after 6w. Scale bar, 2 µm. Asterisks and arrowheads point to nucleus and myelin debris-filled vacuoles, respectively. K) Quantification of number of myelin debris-filled vacuoles per cell (n = 3-4 animals). L-M) Representative images of immunofluorescence F4/80 staining (L) and quantification of the $F4/80^+$ area (M) of the CC from vehicle- and peptide 5A-treated mice after 6w and 6w+1. Scale bar, 200 µm (n = 3-6 animals). Data are represented as mean $\pm$ s.e.m. *, $p<0.05$; **, $p<0.01$; ****, $p<0.0001$.

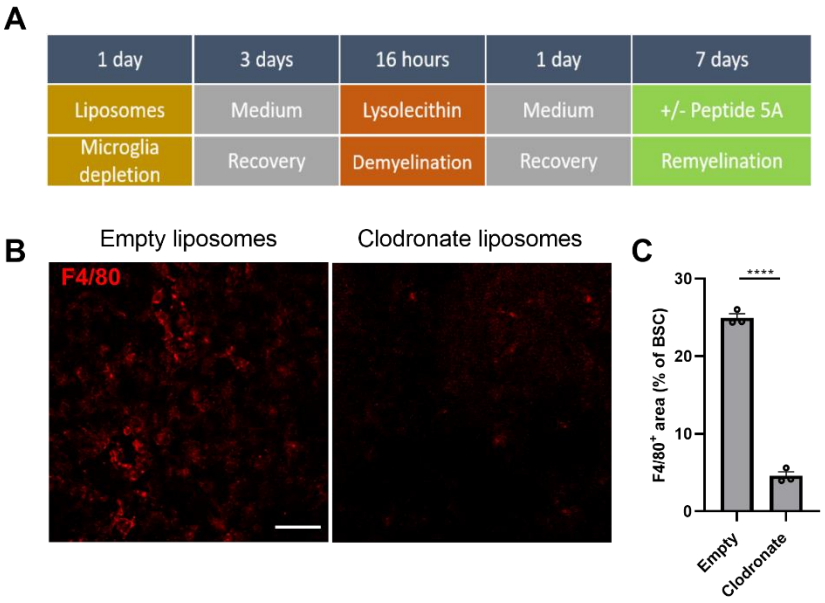

Figure S2: Microglia-depleted brain slice model, related to figure 3. A) Experimental setup of the microglia-depleted cerebellar brain slice model by using empty or clodronate liposomes. B-C) Representative images (B) and quantification (C, n = 3 slices) of immunofluorescence F4/80 staining of cerebellar brain slices treated with empty or clodronate liposomes (0.5 mg/ml) for 24h. Scale bar, 50 µm. ****, p<0.0001.

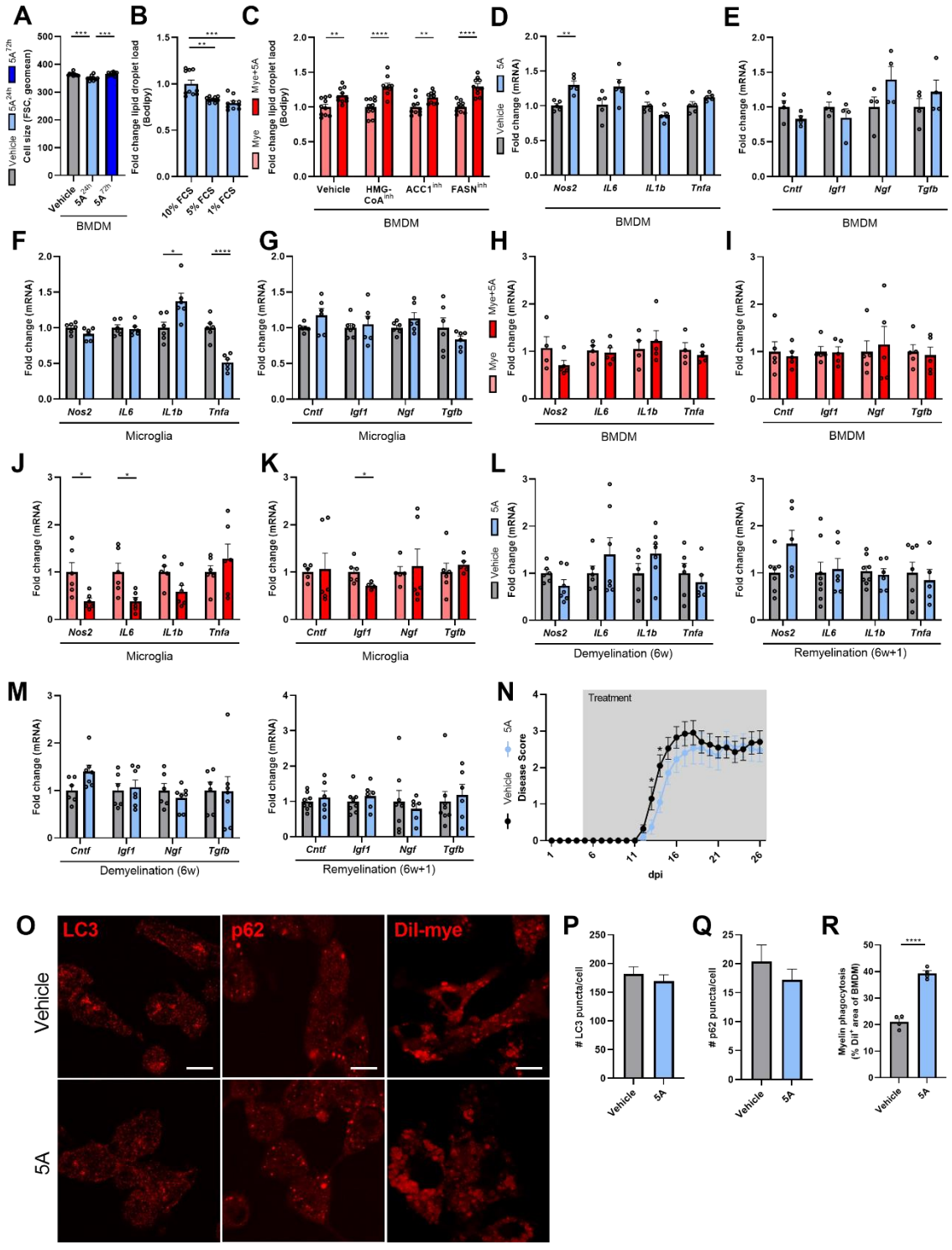

Figure S3: Peptide 5A does not influence cell size, functions independently of de novo lipid synthesis, and does not affect the inflammatory profile and autophagy in macrophages and microglia *in vitro*, related to figure 4. A) Forward scatter analysis, measured using flow cytometry, was used to define the impact of peptide 5A exposure (10 µg/ml, 24h/72h) on cell size of bone marrow-derived macrophages (BMDMs; n = 10). B) Mean fluorescence intensity of BODIPY in BMDMs treated with peptide 5A for 24h and cultured in culture medium supplemented with 10%, 5%, or 1% fetal calf serum (FCS; n = 9-10). C) Mean fluorescence intensity of BODIPY in BMDMs treated with myelin (100 µg/ml) with or without peptide 5A for 72h, and with or without the HMG-CoA reductase inhibitor simvastatin (2 µM), the ACC1 inhibitor TOFA (10 µg/ml) or the FASN

inhibitor C75 (25 µM) (n = 10). D-G) mRNA expression of inflammatory (D, n = 5; F, n = 6) and neurotrophic (E, n = 4; G, n = 6) mediators in BMDMs and microglia treated with vehicle or peptide 5A for 72h. H-K) mRNA expression of inflammatory (H, n = 4-5; J, n = 6) and neurotrophic (I, n = 4; K, n = 6) mediators in BMDMs and microglia treated with myelin with or without peptide 5A for 72h. L-M) mRNA expression of inflammatory (L) and neurotrophic (M) mediators in corpus callosum of vehicle- and peptide 5A (30 mg/kg)-treated mice after cuprizone-induced demyelination (6w) (n = 5-6 animals) and remyelination (6w+1) (n = 5-8 animals). N) Disease score of 12w-old female wild-type mice in which experimental autoimmune encephalomyelitis was induced. Starting 5 days post-immunization, animals were injected intraperitoneally with vehicle or peptide 5A (30mg/kg; n = 10 animals) on a daily basis. O) Representative images of LC3 (left) and p62 (middle) staining, and DiI-myelin-exposed (right) BMDMs treated with vehicle or peptide 5A for 72h. Scale bars, 10 µm. P-Q) Quantification of number LC3 (P) and p62 (Q) puncta per BMDM treated with vehicle (n = 48-56 cells) or peptide 5A for 72h (n = 50 cells). R) Quantification of DiI-myelin$^+$ area per BMDM treated with vehicle or peptide 5A for 72h (n = 4). Results are pooled from two (D-K) or three (A-C, P-R) biological replicates. Data are represented as mean ± s.e.m. *,$p < 0.05$; **,$p < 0.01$; ***,$p < 0.001$; ****,$p < 0.0001$.

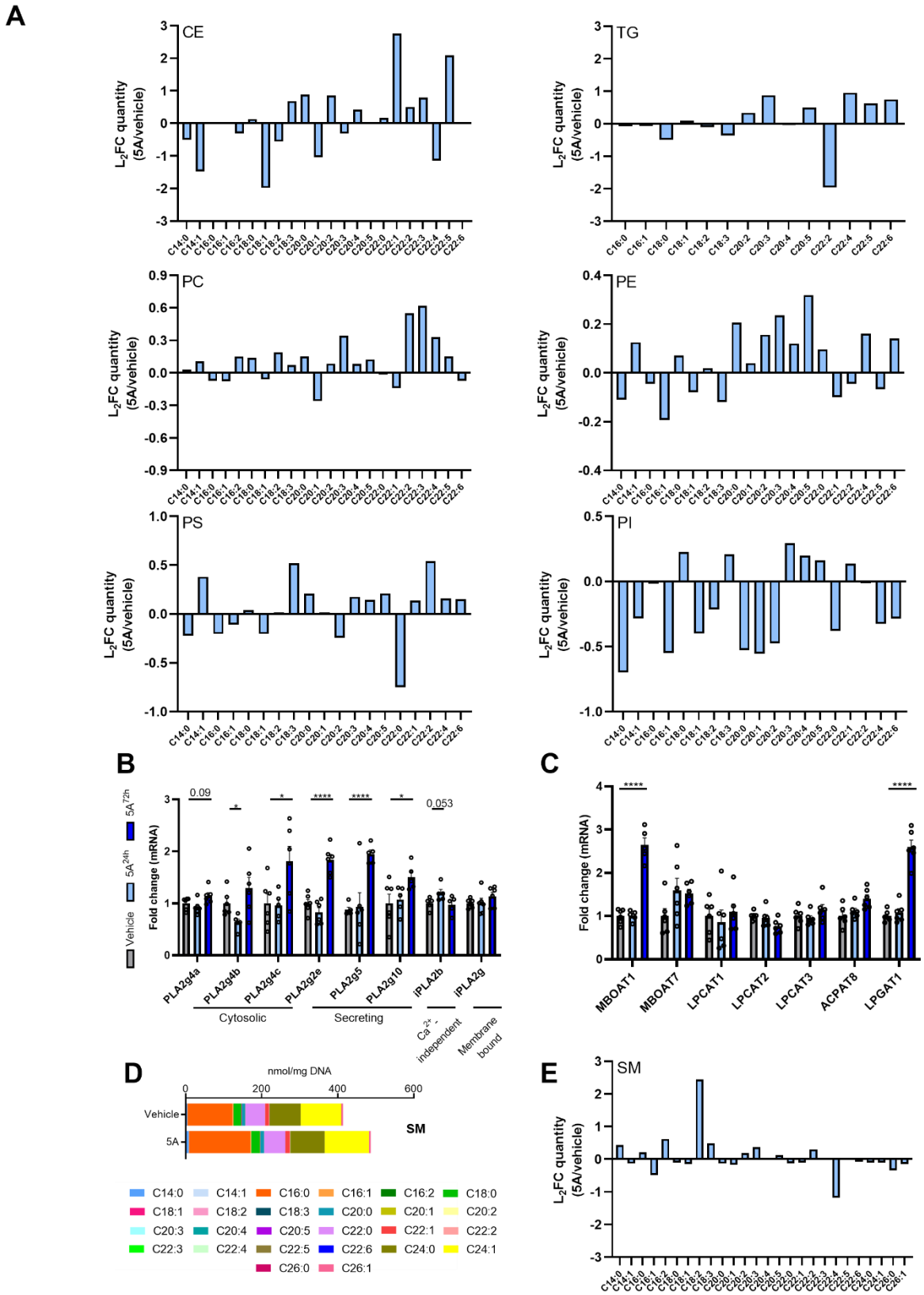
A
CE
TG
PC
PE
PS
PI
L2FC quantity (5A/vehicle)
B
Fold change (mRNA)
Vehicle
5A24h
5A72h
0.09
0.053
PLA2g4a
PLA2g4b
PLA2g4c
PLA2g2e
PLA2g5
PLA2g10
iPLA2b
iPLA2g
Cytosolic
Secreting
Ca2+-independent
Membrane bound
C
MBOAT1
MBOAT7
LPCAT1
LPCAT2
LPCAT3
ACPAT8
LPGAT1
D
nmol/mg DNA
Vehicle
5A
SM
C14:0
C14:1
C16:0
C16:1
C16:2
C18:0
C18:1
C18:2
C18:3
C20:0
C20:1
C20:2
C20:3
C20:4
C20:5
C22:0
C22:1
C22:2
C22:3
C22:4
C22:5
C22:6
C24:0
C24:1
C26:0
C26:1
E
SM

Figure S4: The impact of peptide 5A on lipid metabolism in macrophages, related to figure 6. A) Detailed fatty acid composition of cholesterol esters (CE), triglycerides (TG), phosphatidylcholines (PC), phosphatidylethanolamine (PE), phosphatidylinositol (PI), and phosphatidylserine (PS) of bone marrow-derived macrophages (BMDMs) treated with vehicle or peptide 5A (10 μg/ml) for 72h. Data are depicted as log2 fold change (L_2FC) quantity of peptide 5A-treated BMDMs versus vehicle-treated BMDMs (n = 3). B-C) mRNA expression of genes involved in the hydrolysis (B) and esterification (C) of phospholipids in BMDMs treated with vehicle or peptide 5A for 24h or 72h (n = 5-6). D) Liquid chromatography electrospray tandem mass spectrometry (LC-ESI-MS/MS) analysis of BMDMs treated with vehicle or peptide 5A for 72h. Fatty acid composition of the sphingomyelin (SM) is shown (n = 3). E) Detailed fatty acid composition of SM in BMDMs treated with vehicle or peptide 5A for 72h. Data are depicted as log2 fold change (L_2FC) quantity of peptide 5A-treated BMDMs versus vehicle-treated BMDMs (n = 3). Results are pooled from two (B-C) and three (A, D-E) biological replicates. Data are represented as mean ± s.e.m. *,$p < 0.05$; ****,$p < 0.0001$.

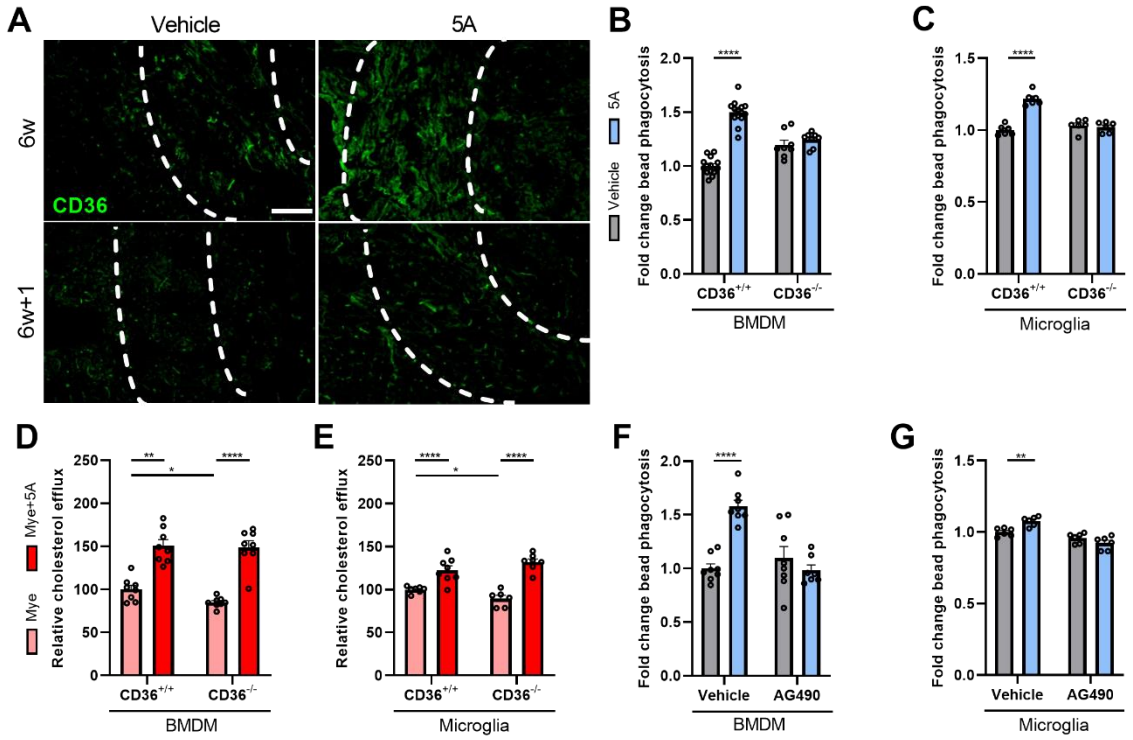

Figure S5: Peptide 5A promotes CD36-mediated bead phagocytosis in a JAK2/STAT3-dependent manner, related to figure 7. A) Representative images of immunofluorescence CD36 staining of the corpus callosum (CC) from vehicle- and peptide 5A (30 mg/kg)-treated mice after cuprizone-induced demyelination (6w) and remyelination (6w+1). Scale bar, 100 µm. B-C) Internalization of fluorescently-labeled beads by wild-type and CD36$^{-/-}$ BMDMs (B; n = 6-14) and microglia (C; n = 6) treated with vehicle or peptide 5A for 72h. Data are depicted as mean fluorescence intensity as defined by flow cytometry. D-E) Relative capacity to efflux cholesterol of CD36$^{+/+}$ and CD36$^{-/-}$ BMDMs (D; n = 8) and microglia (E; n = 8) treated with myelin for 72h and peptide 5A for 4h (50 µg/ml). F-G) Internalization of fluorescently-labeled beads by BMDMs (F; n = 8) and microglia (G; n = 6) treated with vehicle or peptide 5A, with or without the Jak2/Stat3 inhibitor AG490 (25 µM) for 72h (n = 8). Data are depicted as mean fluorescence intensity as defined by flow cytometry. Results are pooled from two (B (CD36$^{-/-}$), C-E, G) or three (B (vehicle), F) biological replicates. Data are represented as mean ± s.e.m. **,$p < 0.01$; ****,$p < 0.0001$.

Table S1: Primer sequences of primers used in the manuscript, related to Figure 1, 2, 5, and 7.

Primer Information	Source	Identifier
Mbp Forward: TCACAGAAGAGACCCTCACAGC	This study	N.A.
Mbp Reverse: GAGTCAAGCATGCCCGTGTC	This study	N.A.
Plp Forward: TTGTTTGGGAAAATGGCTAGG	This study	N.A.
Plp Reverse: GCAGATCGACAGAAGCTTGGA	This study	N.A.
Acat1 Forward: CAGGAAGTAAGATGCCTGGAAC	This study	N.A.
Acat1 Reverse: TGCAGCAGTACCAAGTTTAGT	This study	N.A.
Nceh1 Forward: ATGAGGTCGTCATGCGTCCTA	This study	N.A.
Nceh1 Reverse: TGAAATTCAGCGCGATCAGAT	This study	N.A.
Dgat1 Forward: GTGCCATCGTCTGCAAGATTC	This study	N.A.
Dgat1 Reverse: GCATCACCACACACCAATTCAG	This study	N.A.
Dgat2 Forward: GCTGAGTCCCTGAGCTCCAT	This study	N.A.
Dgat2 Reverse: CAAAGCCTTTGCGGTTCTTC	This study	N.A.
Atgl Forward: TGTGGCCTAATTCCTCCTAC	This study	N.A.
Atgl Reverse: CAGACATTGCCCTGGATGAG	This study	N.A.
Mgat1 Forward: TGGTGCCAGTTTCGTTCCAG	This study	N.A.
Mgat1 Reverse: TGCTCTGAGGTCGGGTTCA	This study	N.A.
Mgat2 Forward: TGGACCCTTCCCGGAACTAC	This study	N.A.
Mgat2 Reverse: TGCACAGGTTAAGAAAGGCTC	This study	N.A.
Hsl Forward: GCTGGGCTGTCAAGCACTGT	This study	N.A.
Hsl Reverse: GTAACTGGGTAGGCTGCCAT	This study	N.A.
Mgl Forward: CAGAGAGGCCAACCTACTTTTC	This study	N.A.
Mgl Reverse: ATGCGCCCCAAGGTCATATTT	This study	N.A.
Lxra Forward: TGTTGCAGCCTCTCTACTTGGA	This study	N.A.
Lxra Reverse: TCTGCAGACCGGCCCAACGTG	This study	N.A.
Lxrb Forward: AAGGACTTCACCTACAGCAAGGA	This study	N.A.
Lxrb Reverse: GAACTCGAAGATGGGATTGATGA	This study	N.A.
Srebp1 Forward: GGAGCCATGGATTGCACATT	This study	N.A.
Srebp1 Reverse: CCTGTCTCACCCCCAGCATA	This study	N.A.
Nos2 Forward: AAAAACCCTTGTGCTGTTCTC	This study	N.A.
Nos2 Reverse: ATACTGTGGACGGGTCGATG	This study	N.A.
Il6 Forward: TGTCTATACCACTTCACAAGTCGGAG	This study	N.A.
Il6 Reverse: GCACAACTCTTTTCTCATTTCCAC	This study	N.A.
Il1b Forward: ACCCTGCAGCTGGAGAGTGT	This study	N.A.
Il1b Reverse: TTGACTTCTATCTTGTTGAAGACAAACC	This study	N.A.
Tnfa Forward: CCAGACCCTCACACTCAG	This study	N.A.
Tnfa Reverse: CACTTGGTGGTTTGCTACGAC	This study	N.A.
Cntf Forward: TCTGTAGCCGCTCTATCTGG	This study	N.A.
Cntf Reverse: GGTACACCATCCACTGAGTCAA	This study	N.A.
Igf1 Forward: TACTTCAACAAGCCCACAGGC	This study	N.A.
Igf1 Reverse: ATAGAGCGGGCTGCTTTTGT	This study	N.A.
Ngf Forward: GGAGCGCATCGAGTTTTGG	This study	N.A.
Ngf Reverse: TCCTTGGCAAAACCTTTATTGGG	This study	N.A.
Tgfb Forward: GGGCTACCATGCCAACTTCTG	This study	N.A.
Tgfb Reverse: GAGGGCAAGGACCTTGCTGTA	This study	N.A.
Mboat1 Forward: AGCCTCTCTTACCGTACCACC	This study	N.A.
Mboat1 Reverse: GGCTGGCTTTACCAGGATGTA	This study	N.A.
Mboat7 Forward: TACCGCACCTACCTGGATTG	This study	N.A.

Mboat7 Reverse: AGAAGACCGGGATCATGTAGAA	This study	N.A.
Lpcat1 Forward: GGCTCCTGTTCGCTGCTTT	This study	N.A.
Lpcat1 Reverse: TTCACAGCTACACGGTGGAAG	This study	N.A.
Lpcat2 Forward: TGTACTAATCGCTCCTGTTTGATT	This study	N.A.
Lpcat2 Reverse: CACTGGAACTCCTGGGATG	This study	N.A.
Lpcat3 Forward: GGCCTCTCAATTGCTTATTTCA	This study	N.A.
Lpcat3 Reverse: AGCACGACACATAGCAAGGA	This study	N.A.
Acpat8 Forward: TTTTATGCTCGGCCCCATTTT	This study	N.A.
Acpat8 Reverse: CACAAGACGGCTGCTAATCCA	This study	N.A.
Lpgat1 Forward: TGGGCTGGATTGTAGCGAAAG	This study	N.A.
Lpgat1 Reverse: CAGATGTAGGATGGAATAGCGAC	This study	N.A.
Pla2g4a Forward: CAGCCACAACCCTCTCTTACTTC	This study	N.A.
Pla2g4a Reverse: CGGCATTGACCTTTTCCTTC	This study	N.A.
Pla2g4b Forward: GCACAAGGACCACTATGAGAATC	This study	N.A.
Pla2g4b Reverse: ACCACCCTAAAAGTGCCCTC	This study	N.A.
Pla2g4c Forward: CACAAACGCAGTCCCAAGG	This study	N.A.
Pla2g4c Reverse: AGACCCCTGCGAGGTATGTG	This study	N.A.
Pla2g2e Forward: CAGTGGACGAGACGGATTCG	This study	N.A.
Pla2g2e Reverse: CAGGTTGTGGCGAAAGCAG	This study	N.A.
Pla2g5 Forward: CTACTGCCTGCCGAGAAACC	This study	N.A.
Pla2g5 Reverse: ACACATCAGGAATACAGCAGAGG	This study	N.A.
Pla2g10 Forward: GAAATACCTCTTCTTCCCCTCC	This study	N.A.
Pla2g10 Reverse: CAGGTGGCTTTAGCACTTGG	This study	N.A.
iPla2b Forward: CGGACGCCTCGTCAACA	This study	N.A.
iPla2b Reverse: CGGAATGGGTTCGAGAACAA	This study	N.A.
iPla2g Forward: CTCTATCGAAAGTTGGGCTCAGA	This study	N.A.
iPla2g Reverse: TCCCACGTGTTACTGTCATAAAAC	This study	N.A.
Lox1 Forward: TCATCCTCTGCCTGGTGTTG	This study	N.A.
Lox1 Reverse: GTCAGATACCTGGCGTAATTG	This study	N.A.
Ldlr Forward: GCATCAGCTTGGACAAGGTGT	This study	N.A.
Ldlr Reverse: GGGAACAGCCACCATTGTTG	This study	N.A.
Cd36 Forward: GGACATTGAGATTCTTTTCCTCTG	This study	N.A.
Cd36 Reverse: GCAAAGGCATTGGCTGGAAGAAC	This study	N.A.
Srb2 Forward: AGCCGACGAGAAGTTCGTTT	This study	N.A.
Srb2 Reverse: CCCGTTTCAACAAAGTCATCCA	This study	N.A.